CURRENT-SOURCE DC-DC CONVERTER FOR FIBER-OPTIC COMMUNICATION SYSTEMS

A Thesis

presented to

the Faculty of California Polytechnic State University,

San Luis Obispo

In Partial Fulfillment

of the Requirements for the Degree

Master of Science in Electrical Engineering

by

Jissell Christine Jose

June 2022

© 2022

Jissell Christine Jose

ALL RIGHTS RESERVED

COMMITTEE MEMBERSHIP

TITLE:	Current-Source DC-DC Converter for Fiber-Optic Communication Systems
AUTHOR:	Jissell Christine Jose
DATE SUBMITTED:	June 2022
COMMITTEE CHAIR:	Taufik, D.Eng. Professor of Electrical Engineering
COMMITTEE MEMBER:	Helen Yu, Ph,D. Professor of Electrical Engineering
COMMITTEE MEMBER:	Majid Poshtan, Ph,D. Associate Professor of Electrical Engineering

ABSTRACT

Current-Source DC-DC Converter for Fiber-Optic Communication Systems

Jissell Christine Jose

In this thesis, a proof of concept for a current-source DC-DC converter for powering sensors used in an underwater communications system is presented. The proposed converter steps down an input current of 0.9 A to 0.625 A, while maintaining an output voltage of 24 V and output power of 15 W. The complete steady-state analysis and design of the proposed converter in its single-stage form is also explained in detail. Performance evaluation of the proposed converter was carried out using LTspice. Results of the simulation demonstrate that the design was able to produce average output current of 0.639 A at maximum output power of 15.292 W while maintaining 24.39 V regulated output voltage. The overall efficiency of the converter was determined to be 88.73% and the output voltage ripple was calculated to be 0.4%, meeting the original specifications of the design.

ACKNOWLEDGMENTS

I am extremely grateful for all the support and guidance I have received that has enabled me to continue my journey of pursing higher education at California Polytechnic State University, San Luis Obispo. First, I would like to thank God for helping me through many of the difficulties I have faced throughout my college education. I am deeply indebted to my parents and loved ones as without their support I would have never been able to achieve my goals. I am grateful for the Newman Catholic Center, Multicultural Engineering Program, Cal Poly Amateur Radio Club, EE/CPE Diversity, Equity and Inclusivity Project, and the Cal Poly Center for Leadership for helping shape me into the person I am today. I would like to extend my sincere thanks to Professor Tina Smilkstein and Marcel Stieber for supporting me in a multitude of ways throughout my undergraduate and graduate studies. I would like to express my gratitude to my thesis advisor Dr. Taufik for his guidance and assistance throughout the development of this thesis as well as inspiring me to explore the subject of Power Electronics. I would also like to thank my committee members for their time, efforts, and participation in my defense.

TABLE OF CONTENTS

Page

LIST OF TABLES

Table Page

LIST OF FIGURES

Figure Page

Chapter 1
INTRODUCTION

From the beginning of time, communication has been one of the most integral parts of human nature. What initially began with sharing information through language has now evolved into the multitude of communication methods present today. Due to the presence of various communication systems, one can find and gather information more rapidly than ever before. A communication system can be defined as a method through which information from a source (the transmitter) is transferred to a destination (the receiver) via a channel (the propagation medium) [1]. One of the primary events in the evolution of communication systems was the development of the electric telegraph. The invention of the telegraph marks the first time that an electronic device was able to successfully communicate text messages faster than physical transportation, which was initially the most common method to share information. From this point forward, communication systems have expanded with the development of the telephone, phonograph, radio, television, internet and more. Society depends heavily on the various communication systems in place ranging from making quick phone calls to gathering data from satellites thousands of miles away.

One innovation in the development of communication systems has been the creation of optical fibers and fiber-optic communication systems. An optical fiber is a thin piece of flexible glass that can transmit light from one end to another with minimal loss in strength. Optical fibers can then be bundled together to create fiber optic cables. Optical fibers can be used as sensors, as devices for power transmission, and most commonly as apart of fiber optic communication systems [2]. Fiber optic communication

systems transmit information from one location to another by sending pulses of infrared light through optical fiber. The infrared light behaves as a carrier wave that is then modulated to carry information. Since its development, fiber optics has become the predominant communication medium. Some common applications for fiber optics include both mobile and wireless telephones, Internet, cable television, computer networks, surveillance/security systems, industrial controls, traffic signals, utility grid communications and control, energy exploration/production, alternative energy and more [2]. Fiber-optic communication systems are widely used today as they can transmit high bandwidth voice, video, and telemetry data over long distances; and are preferred over electric cabling in these instances. Another very common use of fiber optic technology can be found in undersea communication systems which create communication links between continents or other landmasses.

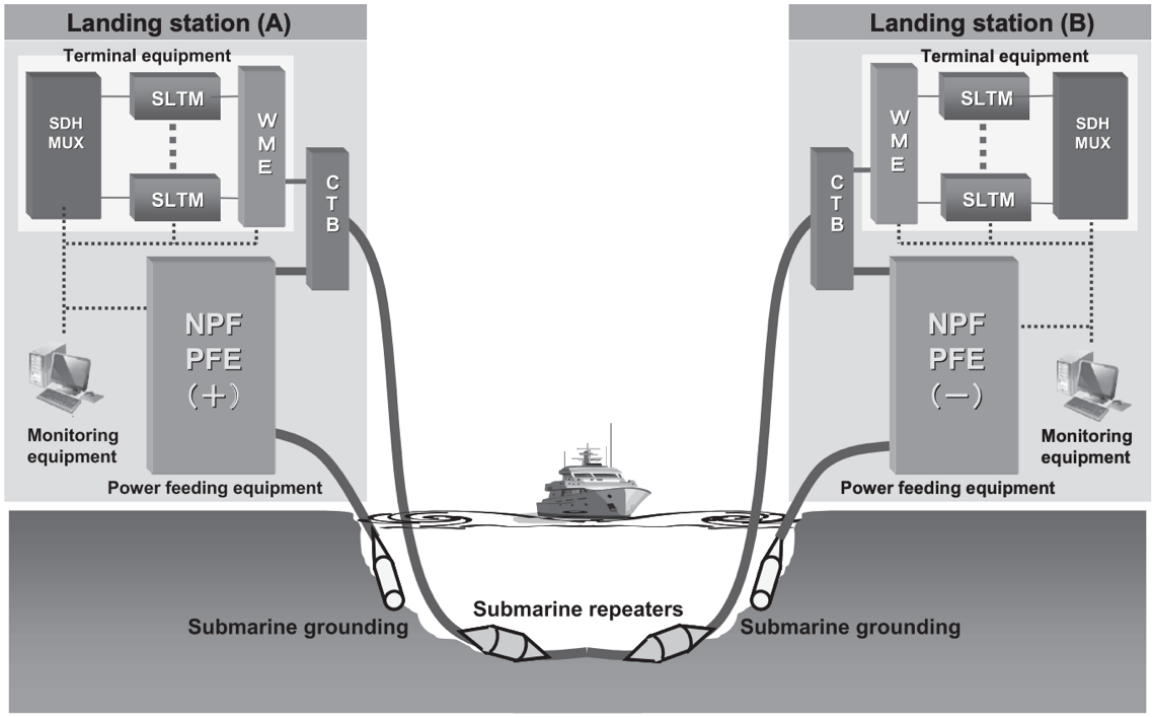

Figure 1-1: Standard Submarine Cabling System [3]

There are several major components of undersea fiber optic systems as illustrated in Figure 1-1. One of the primary components is the undersea fiber optic cable. It is made up of multiple pairs of fibers which are coated in layers of metal and composites for protection. The sizing of the cable depends upon the depth of the seabed where the cable is placed, as depicted in Figure 1-2.

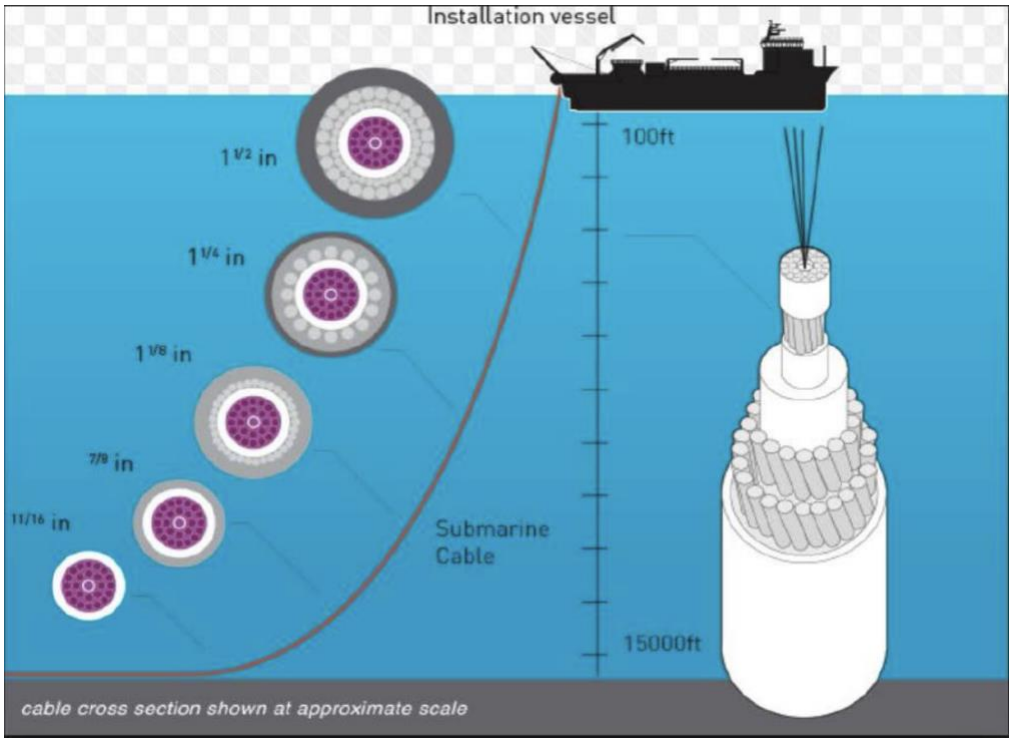

Figure 1-2. Sizing of Optical Undersea Fiber Optic Cables Based on Ocean Depth [4]

Large amounts of current and voltage travel through these cables, which is produced by power feed equipment, or PFE. PFE is placed at terminal stations on land and produces large amounts of voltage for the line. Some of the primary requirements of PFE include high reliability to avoid interruption of active communication line, stable current feeding, protection functions to avoid overcurrent and overvoltage, high conversion efficiency from primary source to output power, and protection for individuals preforming maintenance due to the dangerous high voltages produced by PFE

equipment [5]. The cable landing point is the location from which the cable transitions from sea to land and the cable ends at a termination station where the cable connects to a terrestrial network [6].

Another important aspect of the system are repeaters. Repeaters are utilized within the communication system to regenerate the infrared light wave across the body of water. These are integral to the system as optical signals can only travel between 100-400 km [6]. Figure 1-3 shows that these repeaters are housed within a capsule to protect the electronic components inside and are placed every 50-100 km within a system. A repeater is comprised of a cylindrical pressure housing, typically 300-360 mm in diameter and from 600 to 1200 mm long and contains internal components, couplings, bell housings, and bend limiters [7].

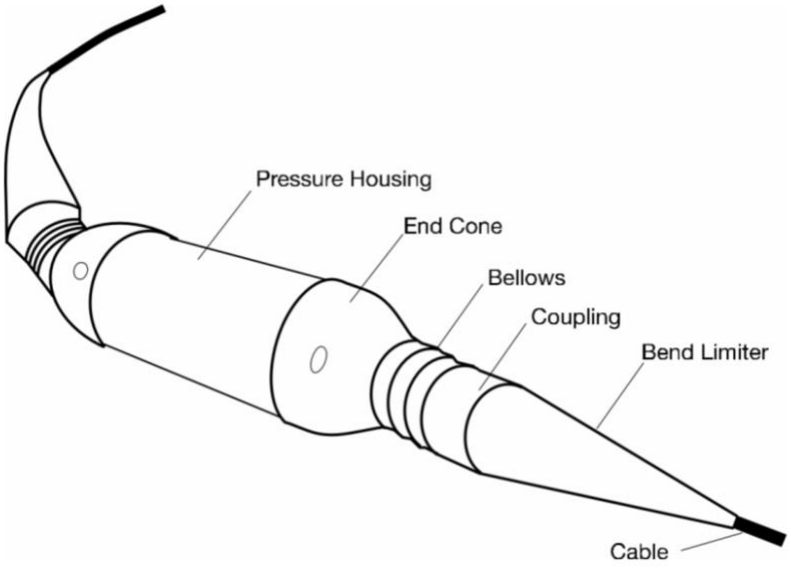

Figure 1-3. Standard Design of Submarine Telecommunications Repeater [7]

Undersea fiber optic communication systems also utilize sensors used to gather data about the communication system and its surroundings. The data from these sensors can also be utilized to provide information about climate change and even have the

potential to provide early warnings about earthquake and tsunami events [7]. Some of the most used sensors include temperature and pressure sensors. There are two primary methods utilized to place sensors into the system. One method integrates the sensors into the repeater housing. This method is convenient as all components in the system will be placed in one location. In this case, the repeater housing must be large enough to accommodate the sensors and any other components that are needed for its operation. Furthermore, overheating is more likely to become an issue in this method and utilizing heatsinks and components with high temperature ratings within the design is very important [7]. The second option is utilizing an external pod alongside the repeater where the sensors are placed. This method has the advantage of moving the temperature sensor away from any heat dissipated by the repeater. The disadvantage of this method is that it would require additional power conductors and optical fibers to connect from the repeater housing to the sensor pod. Figures 1-4 and 1-5 illustrate the inside repeater and inside external pod sensor mounting methods, respectively.

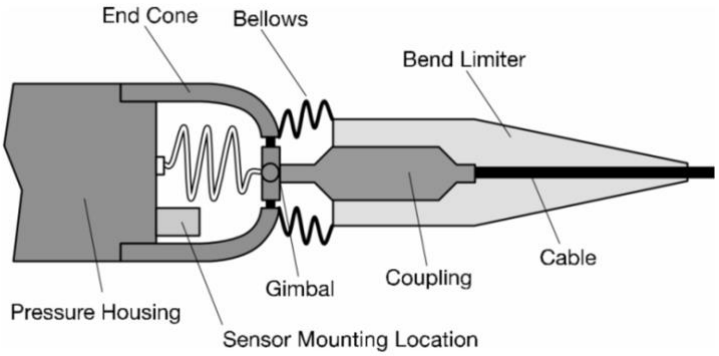

Figure 1-4. Example of Sensor mounting inside repeater [7]

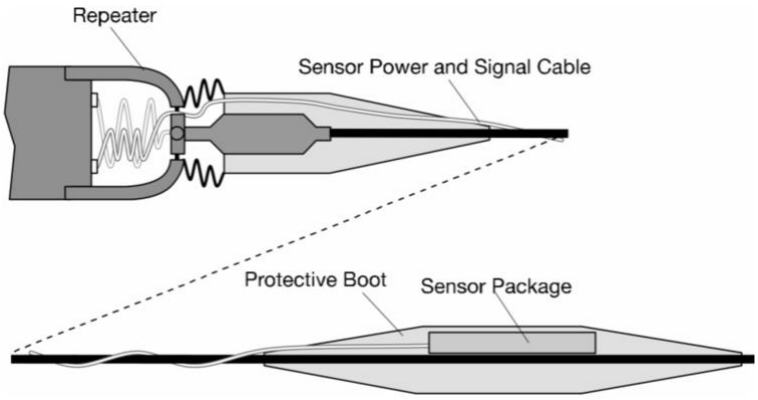

Figure 1-5. Example of Sensor mounting inside external pod [7]

To utilize the sensors within an underwater capsule, a DC-DC power supply is needed to power the system. This power supply must be able to convert the large amounts of voltage and current that move through the communication system to more manageable amounts. Without this conversion process, the sensors would overheat and inoperable. To achieve this goal while maintaining efficiency within the system successfully, the utilization of power electronics becomes a necessary tool. Power electronics can be defined as the study of processing the flow of electric energy efficiently by controlling semiconductor devices to meet load users or user requirements [8].

Chapter 2
BACKGROUND

Power electronics enables the user to control the flow of voltage and current in a system by converting it into a form that can meet the load or user requirements. The four primary categories of power electronic converters consist of AC-DC, AC-AC, DC-AC and DC-DC converters. Power electronic systems are utilized in a wide range of applications as most electrical energy conversions today are performed by power electronics. This makes the study of power electronics and innovation in this field essential for the future. Some of the important factors related to the design of power electronics systems include efficiency and reliability. Efficiency is defined as the ratio of average output power to average input power, with higher efficiency values indicating that minimal power is wasted within the system as heat or other losses. The reliability of a device determines if it will continue to operate as desired during less-than-optimal conditions, impacting the lifespan of the device.

Efficiency of the system is an important factor as it directly relates to energy usage of the system; thus, it would impact the operating cost of the system. Efficiency is also crucial when minimizing the physical size of the system is a priority. Efficient system means very little power loss occurs in the system which will further implies the use of small components or avoid the use of cooling system which adds cost to the overall system. As for reliability, depending on the application of the system and environment where it is used, a large variety of stressors can endanger the safe operation of components. These stressors can severely impact the reliability of the system, which

can result in potentially dangerous situations for the end users. Some examples of stressors include high temperatures, pressure, temperature cycling, vibrations, electromagnetic interference, and radiation [9]. The presence of these stressors can impact the safe operation of the many fragile components found in electrical systems which can include electronic devices, capacitors, inductors, controllers, and various sensors. As a result, every component chosen for a system must be able to withstand any of the potential stressors it may encounter.

As mentioned previously, one type of power electronic converter is known as a DC-DC converter. DC-DC converters are utilized when a primary DC source needs to deliver power several different components which require a DC voltage that is different from the source. The output voltage and current of a DC-DC converter can be made higher, lower, or equal to than that of the input values based upon which circuit or topology is being used. Switch mode DC-DC converters utilize solid state switches in their operation and deliver power by storing the input energy temporarily and then releasing that energy to the output at a different voltage or current. For example, when a specified switch is closed, the source provides power to the load while also charging energy storage components. When the switch is opened, the source becomes disconnected from the load, causing the energy storage component to discharge and supply power to the load [10]. A feedback controller can also be added to the converter to minimize the error between a reference value to the actual output value. As a result, by alternating between states and employing a feedback controller, a DC-DC converter can deliver power efficiently and produce a constant output voltage and current.

To determine the performance of a DC-DC converter, measurements of efficiency, voltage ripple, line regulation, load regulation can be conducted through simulations and experimental testing [8]. Line regulation is calculated to determine how a change in input voltage can affect the output voltage of the converter. Line regulation is calculated using equation 2-1 in which Vout (max), Vout (nominal) and Vout (minimum) are the average output voltages measured at full load when the maximum, nominal and minimum input voltages are applied to the system, respectively.

$$Line\ Regulation = \frac{Vout\ (\max) - Vout\ (min)}{Vout(nominal)} \tag{2-1}$$

Load regulation determines how changing the loading (output current) of the circuit can affect the output voltage of the converter. Load regulation is calculated using equation (2-2) in which Vout (10%) and Vout (90%) are defined as the average output voltages measured at 10% loading and 90% loading, respectively.

$$Load\ Regulation = \frac{Vout\ (10\%) - Vout\ (90\%)}{Vout(90\%)} \tag{2-2}$$

Going back to the two methods in mounting the fiber optic sensors as mentioned in the previous chapter, in the case of fiber optic sensors housed within submarine repeater capsules, the amount of voltage applied to the sensors must be stepped down significantly. Within underwater communication systems, a high voltage (1000V-5000V) is supplied from the power source to transfer the data through long lines of fiber optic cable. If this voltage was then immediately applied to the sensors, they would be damaged as these components are not rated to handle the extremely high amounts of

voltage. There are at least two types of DC-DC converter solutions that may be used to address this problem: voltage-fed or voltage-source topologies and current-fed or current-source topologies. Voltage-source topologies are fed with a constant voltage at the input while current-source topologies are fed with a constant current at the input.

2.1 Comparison of Voltage-Source and Current-Source DC-DC converters

The primary difference between these two topologies is their energy storage method. Voltage-Source DC-DC converters utilize capacitive storage methods while current-fed converters utilize inductive storage methods within their design. Voltage-Source converters are the more widely used topology as power supplies with consistent voltage output are often used as a source, making this topology seem like the most intuitive design choice. However, when there are multiple loads in the system each requiring different amounts of power and voltage, this may not be the most ideal method. A long distant transmission of power could also pose a technical issue for the voltage-fed topologies. In the case of the underwater repeater system, if there are multiple submarine repeaters placed in series and spaced out with a significant distance between each other, then each repeater will have a different input voltage. Depending on how much this voltage varies, each voltage-controlled DC-DC converter on every repeater could potentially need to be redesigned to handle the input voltage. In the case of a Current-Source DC-DC converter, the input current would not change based upon the number of repeater modules placed in series as well as distance between one another and the feeding power supply. This makes input current to be a more consistent variable compared to the

input voltage. Figures 2.1 and 2.2 show examples of simplified schematics both converters.

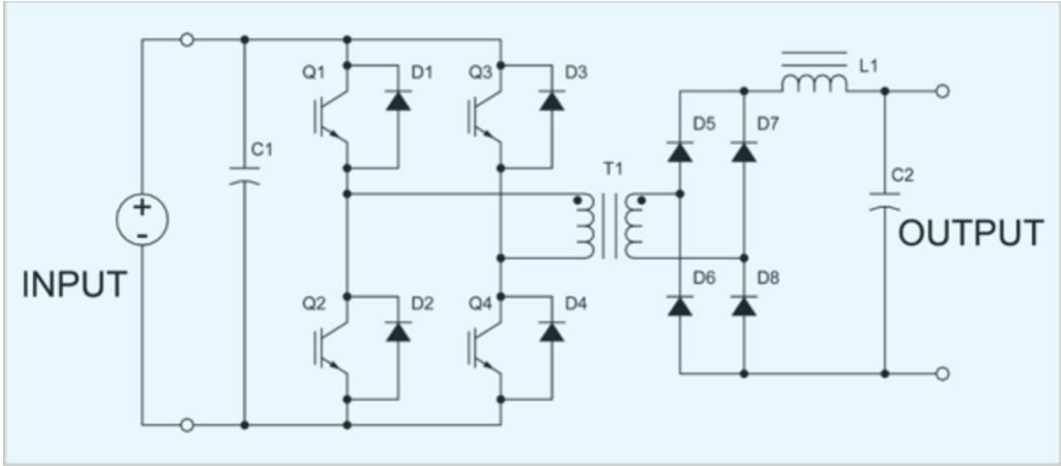

Figure 2-1. Example of a Voltage-Source DC-DC converter [11].

A simplified schematic of a voltage-fed converter is shown in Figure 2.1 The converter consists of an H-bridge, power transformer T1, and output rectifier diodes D5 to D8 [11]. Examples of input voltage sources can be a battery, DC power supply or rectified AC bus. Capacitor C1 is needed to allow for a low impedance bus at higher frequencies. Inductor L1 and capacitor C2 form a low-pass filter which removes the AC components on the output. If Q1 and Q2 or Q3 and Q4 conduct simultaneously, current rapidly rises in the conducting devices leading to failure in microseconds. As with standard Pulse Width Modulation (PWM), Q1 and Q4 conduct for a half-cycle while Q2 and Q3 conduct for the other half-cycle, exciting the transformer T1 equally on alternate half-cycles [11]. By averaging the rectified voltage on the secondary side of the transformer, a DC output voltage is produced that is proportional to the conduction period of the H-bridge.

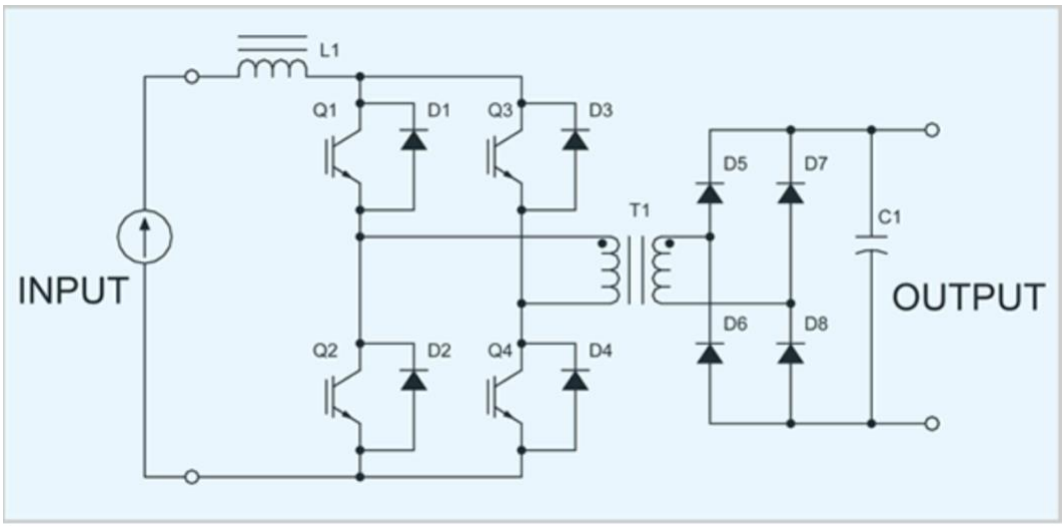

Figure 2-2. Example of a Standard Current-fed DC-DC converter [11].

As shown in Figure 2-2, the standard current-fed converter consists of an H-bridge, power transformer and output rectifier diodes. Inductor L1 is needed to allow for a high impedance bus at higher frequencies. Unlike the voltage-fed converter, the output filter consists of a single component, capacitor C1. In current-fed converters, voltage and current waveforms are transposed from that of voltage-fed converters [11]. Operation requires switches Q1 to Q4 to be PWM-modulated, but in this case, Q1 and Q3 or Q2 and Q4 are never allowed to be simultaneously placed in a non-conducting state. This constraint allows for input impedance of the H-bridge to always be finite; otherwise, a current source feeding into an open current would produce a destructive high voltage [11]. By averaging the rectified current on the secondary side of the transformer, the DC output current produced is proportional to the conduction period of the H-bridge. The transformer utilized in the design is not affected by variations of on-state voltages, varying rise and fall times, and erroneous switching states. With current-fed converters, one concern is core saturation which is preventable if the ampere-turn excitation is within the bounds of normal operation, even for a DC current [11]. The comparison of the

voltage-fed and current-fed DC-DC converters indicate that depending on the type of application, it is worthwhile to look at both types of converters and determine which can provide the best results for the end user.

2.2 Voltage-Source Topology Example

One example of a step-down DC-DC converter utilizing a voltage source for fiber optic sensors is presented in [10]. The converter steps down an 5000V-6000V input to a 24V output, which powers the input to sensors located in a submarine repeater capsule. The completed system consists of two stages where the first stage is an unregulated switched capacitor converter to step down the initial input to a voltage range more appropriate for the selected second stage [10]. The second stage is a regulated flyback converter topology which regulates the final output to the desired 24V. Stage 1 utilizes a 4^{th} order exponential switch capacitor (ESC) topology as it provides a high gain conversion ratio of $1/16^{th}$ and can maintain efficiency when voltage regulation is not a necessity. Stage 2 on the other hand utilizes a flyback converter topology to efficiently step down the voltage from the first stage to the desired value of 24 V [10]. Figure 2-3 shows the schematic of the proposed step-down voltage-fed DC-DC converter. The design was simulated in LTSpice and yields an efficiency of approximately 74.95% when tested under nominal input and full load conditions. With the same conditions, the converter yields an output voltage ripple of 1.525%, and line and load regulations of 0.0457% and 0.183% respectively [7]. The results of this paper show that the proposed design was able to meet a majority of the requirements of the system, with only a slightly lower efficiency than desired.

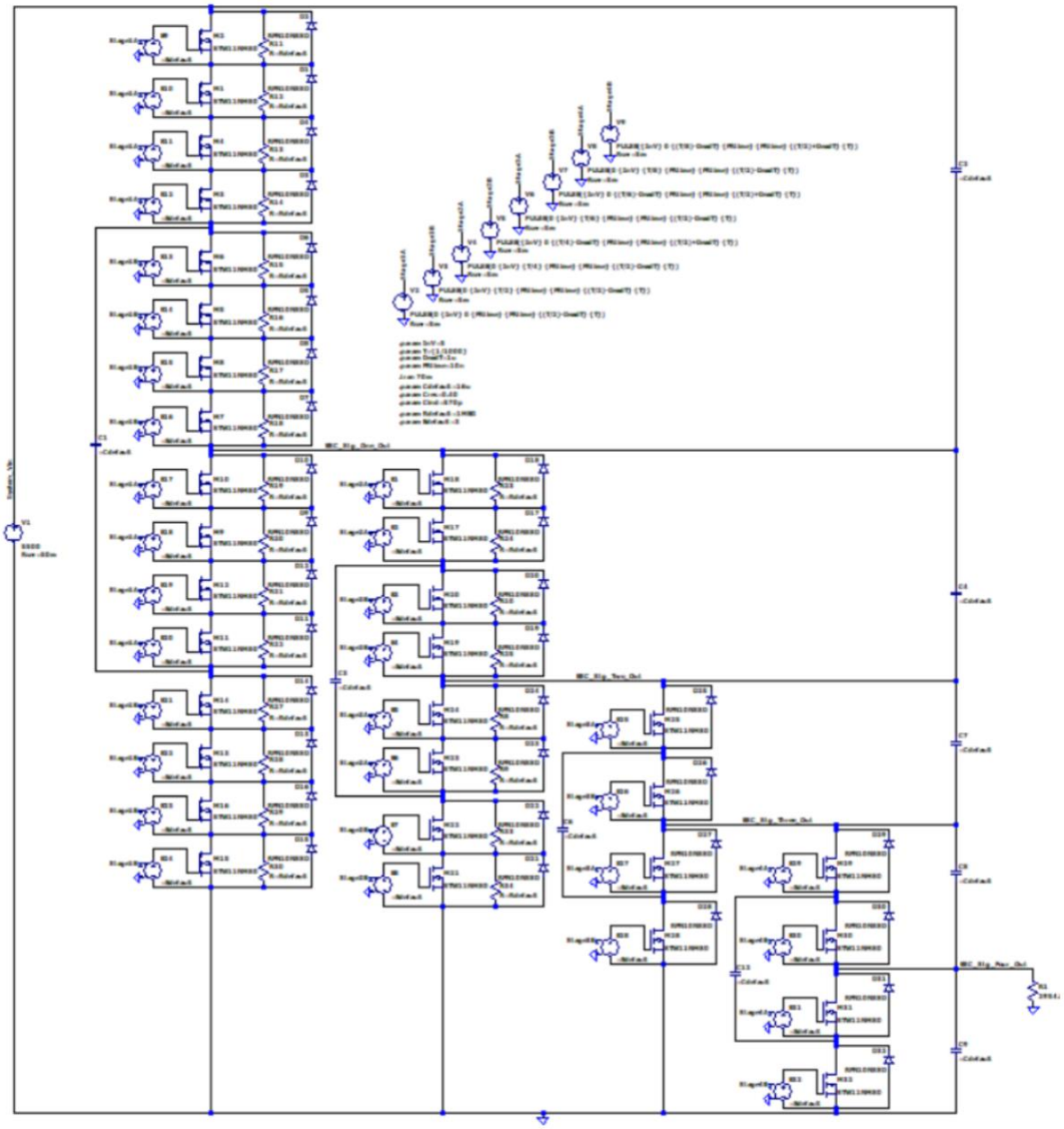

Figure 2-3. System Stage One 4th Order ESC LTSpice Simulation Model [10].

2.3 Current-Source Topology Example

One example of a Current-Source DC-DC converter developed to step down voltage was presented in [12]. In this paper a current-source converter for use in photovoltaic systems was proposed and simulated in EMTDC/PSCAD software.

Photovoltaic systems require power electronic converters as they act as the interface between input sources and the load to generate desirable outputs. In this topology, zero current switching of primary-side devices and zero voltage switching of secondary-side devices are obtained [12]. This minimizes switching losses as well as voltage and current stresses on power electronic devices.

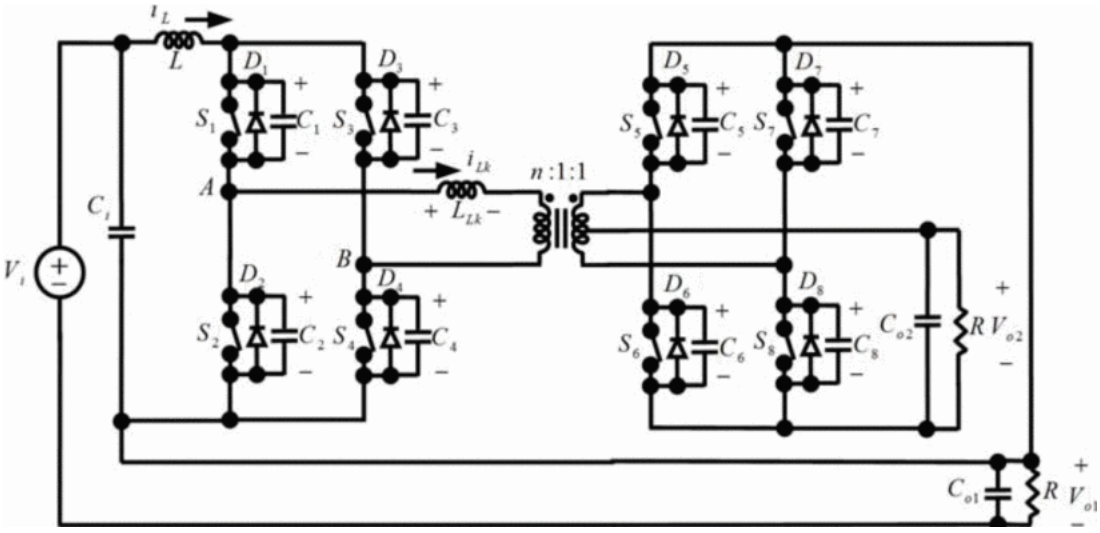

Figure 2-4. Dual-output step-down soft switching current-fed full-bridge DC-DC converter [12].

In this current-fed converter design, diodes D1- D8 are the internal diodes of switches S1-S8 and capacitors C1-C8 represent the parasitic capacitor of switches S1 - S8. The duty cycle of switches S1-S4 must be greater than 50% while the duty cycle of switches D5-D8 must be less than 50% [12]. The input inductor L decreases the input current ripple. The leakage inductance, L_{LK}, and parallel parasitic capacitors with the switches provide soft switching operation. In this design, C_{01} and C_{02} are output filter capacitors and dual-outputs for the design are provided using a three-winding transformer on the secondary side. In this topology, after turning on the pair of switches S1 and S4 on

the primary-side as well as S6 and S7 on the secondary-side, the other pairs (S2 and S3) and (S5 and S8) are turned off [12]. Reflected output voltage nV_{02} is created across the transformer primary, increasing the current through switches pair, while reflected output voltage $-nV_{02}$ is created across the transformer primary, decreasing the current through the switches pair [12]. As a result, the current of switches on the primary side reaches to zero with ZCS and the commutated device capacitance starts to charge.

Simulations of the design were performed after analysis of the 8 operation modes of the circuit was completed. Calculations of the voltage gain for both outputs as well as equations for the sizing of the inductors to be utilized in the design were determined through circuit analysis. In the simulation the duty cycle utilized on the primary side was 0.67 with a transformer turns ration of 8:1:1. With an input voltage of 48 V, this design was able to step the voltage down to 15.5 V on output V_{01} and 7.54 V on V_{02}, which were very similar to the calculated values of 13.76 V and 6.89 V, respectively.

The analysis of voltage-source and current-source DC-DC converters lead to the objective of this thesis which relates to the Indonesian Cable-Based Tsunameter (Ina-CBT) project that is currently underway by the Agency for the Assessment and Application of Technology in Indonesia. More specifically, this thesis aims to study, design, and analyze a current-source DC-DC converter to power underwater sensors that operate with low level DC electricity found within underwater repeater capsules.

Chapter 3
DESIGN REQUIREMENTS

3.1 Electrical Specifications

As previously stated, the objective of this thesis is to study, design, and analyze a current-source DC-DC converter for powering submarine sensors. The converter will receive maximum input voltage of 1500 V DC and input current of 0.9 A with a tolerance of ±5%. The converter must then transform the voltage to 24 V DC output voltage with ±2% tolerance and output current of 0.625 A. This translates to the rated output power of 15W to operate the sensors housed within the submarine repeater. Since this is a current-source converter, the amount of current input to the system is extremely important, as this determines key factors within the converter design as well as the power rating of the PFE power supply. Figure 3-1 illustrates a high-level depiction of the proposed DC-DC current fed converter.

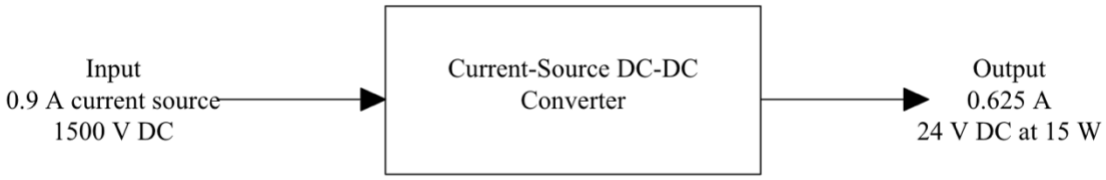

Figure 3-1. System Level 0 Block Diagram.

The current-source DC-DC converter should also utilize a feedback controller. This feedback controller is placed in the system to help maintain the output voltage at a constant value of 24 V DC if there is a sudden change in the input current or voltage as well as the output current. The addition of the feedback controller is shown in Figure 3-2.

To minimize the amount of heat dissipation in the converter, the efficiency of the proposed converter should be at least 80% at full load.

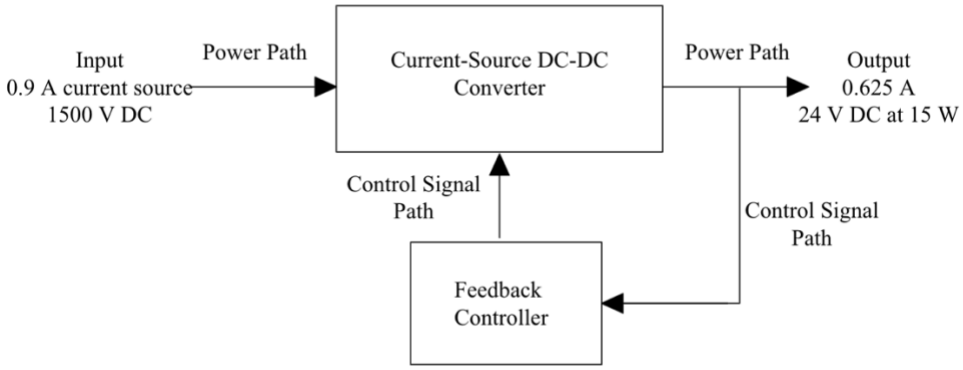

Figure 3-2. System Level 1 Block Diagram.

3.2 Physical Specifications

The converter will be placed within a pressurized vessel that will be deployed within the underwater system. This vessel has a cylindrical shape and is made from a copper material with a length of 80 cm and a diameter of 22 cm. As a result, the proposed current-source DC-DC converter must be designed on a circuit board that fits within the vessel. Figure 3-3 is a diagram that illustrates the physical dimensions of the vessel.

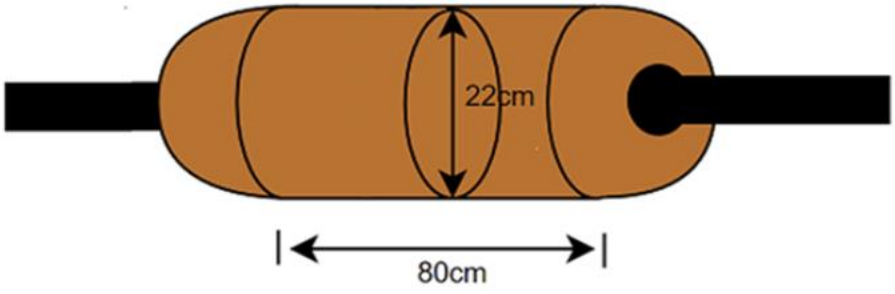

Figure 3-3. Submarine Housing of DC-DC Converter [10].

Table 3-1 summarizes both the electrical and physical specifications discussed previously for the proposed current-source DC-DC converter to meet the requirements of the end user.

Table 3-1. Summary of System Requirements for Current-Source DC-DC Converter.

Specification	Value
Converter Electrical Specifications	
Maximum Input Current	0.9 A
Average Output Voltage	24 V DC
Maximum Output Current	0.625 A
Output Voltage Ripple	< 2%
Maximum Output Power	15 W
Overall Efficiency	≥ 80%
Converter Physical Requirements	
Length	≤ 80 cm
Width	≤ 20 cm

Chapter 4

SYSTEM DESIGN

The proposed converter design should be able to convert an input current of maximum 0.9 A to a regulated output voltage of 24 V at full load current of 0.625 A. This translates to maximum output power of 15 watts. The proposed current source DC-DC converter should utilize an isolated topology with a full bridge inverter on the primary side for maximum transformer utilization and a rectifier on the secondary side to obtain the DC output voltage. To maintain a 24 V output voltage, a closed-loop feedback system must be implemented with a voltage divider network being used as the output voltage sensor to scale down the output voltage to a level manageable by the controller circuitry. The level 2 system diagram illustrating the system is shown in figure 4-1.

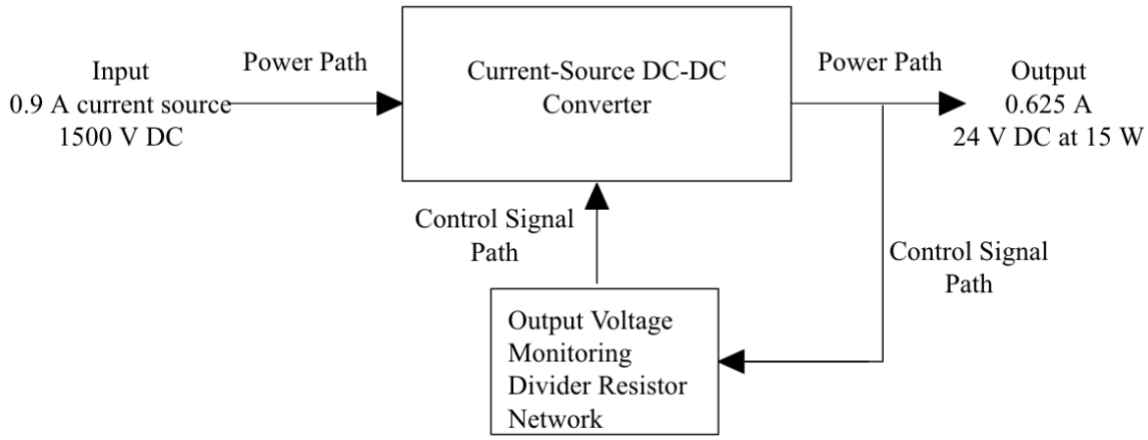

Figure 4-1. System Level 2 Block Diagram.

4.1 Steady State Analysis of Current Source DC-DC Converter

The power stage of the proposed Current Source DC-DC Converter can be understood and modeled by the simplified current source DC-DC converter illustrated in

Figure 4-2. In this example the constant current at the input is represented by the constant current flowing through the large inductor L found at the input. This inductor is needed to mathematically assign voltage across the inductor, which allows one to derive the converter's transfer function. The input voltage $\bar{V}_{in}$ can vary depending on the output current I_{out} chosen for the design.

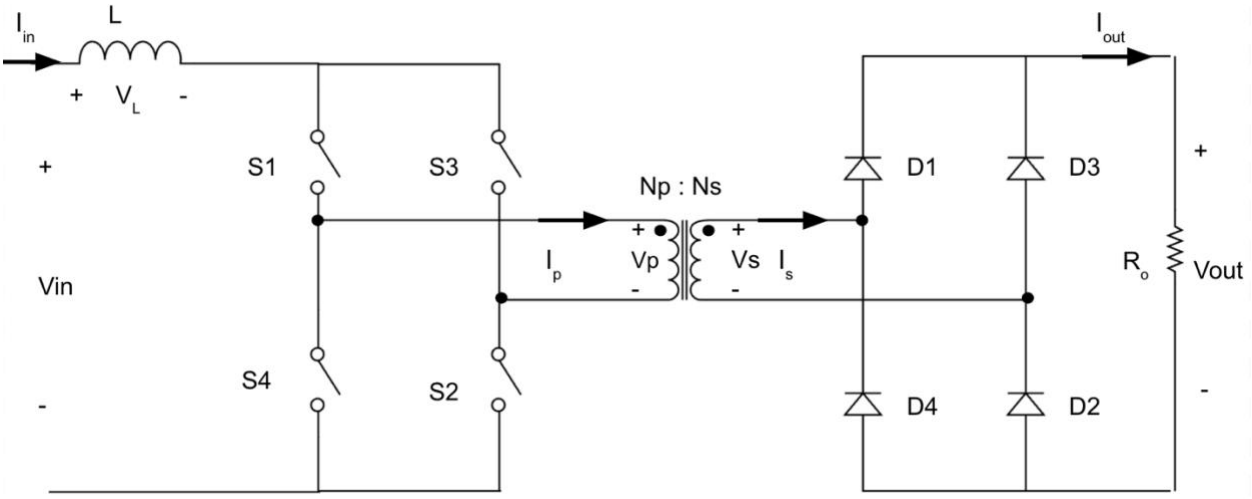

Figure 4-2. Simplified Current Source DC-DC converter.

Using Figure 4-2, the steady state transfer function of the converter can now be derived. To determine the transfer function, it is assumed that all components in this design are ideal. The second assumption is that the load R_o is drawing constant power or current. This assumption allows us to determine that V_{in}, the input voltage will remain constant. This converter has a total of 3 states in the circuit steady state operation, which are then used to derive the transfer function. In the first state, switches S_1 and S_2 are on while switches S_3 and S_4 are off. In the second state, switches S_1 and S_2 are off while switches S_3 and S_4 are on. In the third and final state, all four switches remain on. Each of these states will be analyzed accordingly.

4.1.1 State 1: S_1 and S_2 are on, S_3 and S_4 are off

During this state, the secondary current flows through diodes D_1 and D_2. The equivalent circuit for this state is shown in Figure 4-3. In this case, the transformer's secondary winding voltage (V_s) can be determined from equation 4.1 while the voltage across the inductor in state 1 ($V_{L_{on1}}$) can be calculated from equation 4.2, which uses the relationship between the secondary winding voltage with the output voltage and turns ratio as shown in equation 4-1.

$$V_s = \bar{V}_{out} = V_p \frac{N_s}{N_p} \rightarrow V_p = \frac{N_p}{N_s} \bar{V}_{out} \tag{4-1}$$

$$V_{L_{on1}} = \bar{V}_{in} - V_p = \bar{V}_{in} - \frac{N_p}{N_s} \bar{V}_{out} \tag{4-2}$$

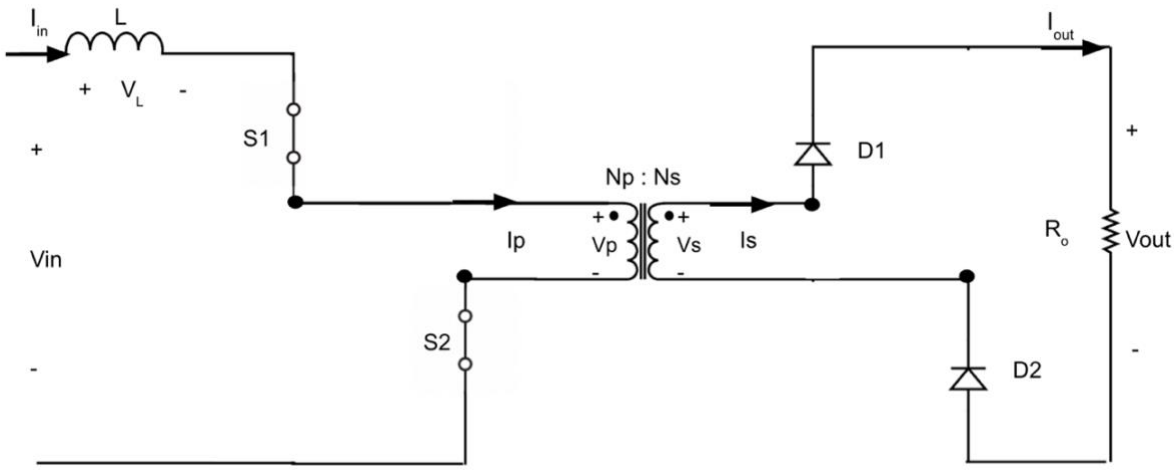

Figure 4-3. Equivalent Circuit of State 1.

4.1.2 State 2: S_1 and S_2 are off, S_3 and S_4 are on

During this state, the secondary current flows through diodes D_3 and D_4. The equivalent circuit for this state is shown in Figure 4-4. In this case, the transformer's secondary winding voltage (V_p) can be determined from equation 4-3 while the voltage across the inductor in state 2 ($V_{L_{on2}}$) can be calculated from equation 4-4, which uses the relationship between the secondary winding voltage with the output voltage and turns ratio.

$$V_s = -\bar{V}_{out} = -V_p \frac{N_s}{N_p} \rightarrow V_p = \frac{N_p}{N_s}\bar{V}_{out} \tag{4-3}$$

$$V_{L_{on2}} = \bar{V}_{in} - V_p = \bar{V}_{in} - \frac{N_p}{N_s}\bar{V}_{out} \tag{4-4}$$

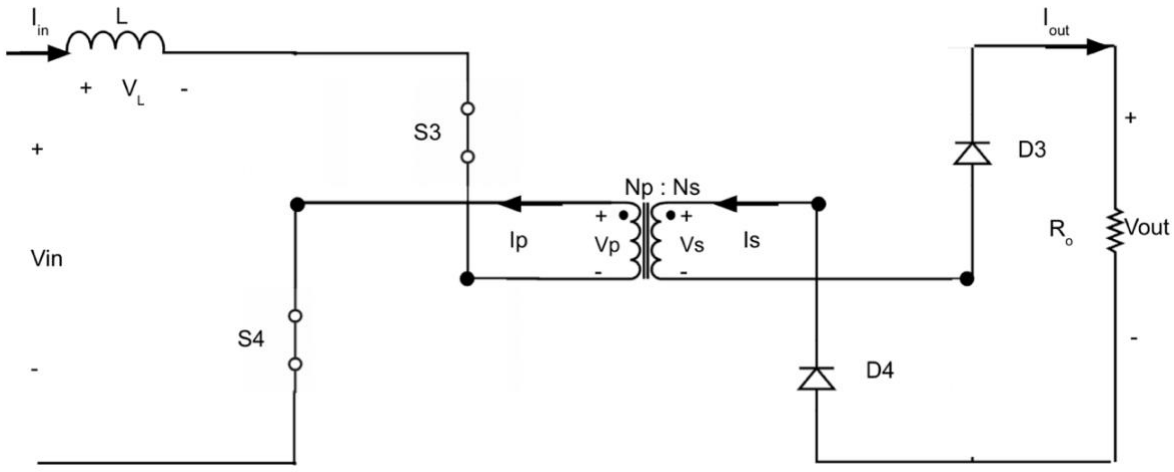

Figure 4-4. Equivalent Circuit of State 2.

4.1.3 State 3: All Switches are on

During this state, the primary winding is shorted as illustrated in the equivalent circuit of state 3 in Figure 4-5. Since the primary winding is shorted, no energy is transferred to the load. This occurs as no current is reflected on the secondary side of the transformer, causing diodes D_1-D_4 to remain in a non-conducting state.

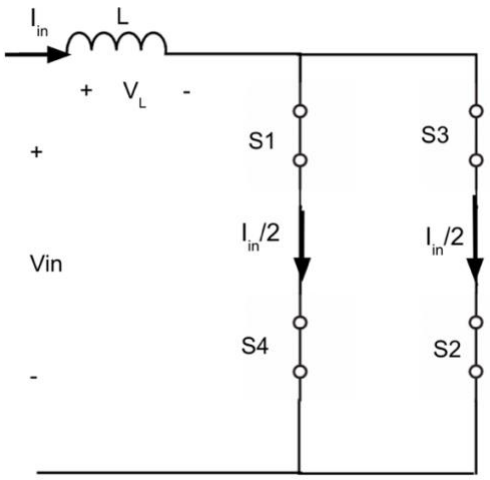

Figure 4-5. Equivalent Circuit of State 3.

Furthermore, the voltage across both the primary and secondary sides of the transformer is equal to zero due to the short circuit. This causes the voltage across the inductor in state 3 ($V_{L_{on3}}$) to be equivalent to the input voltage ($\bar{V}_{in}$), which can be used to determine the voltage transfer function of the converter. One must also know the on time (t_{on}) and off time (t_{off}) of the converter, which is calculated utilizing information from the inductor voltage waveform shown in Figure 4-6. This figure shows how the voltage across the inductor relates to the duty cycle (D) and the period (T). For the current-source DC-DC converter to operate, the duty cycle must be between 0.5 and 1. The calculations for t_{on} and t_{off} can be seen in equations 4-5 and 4-6.

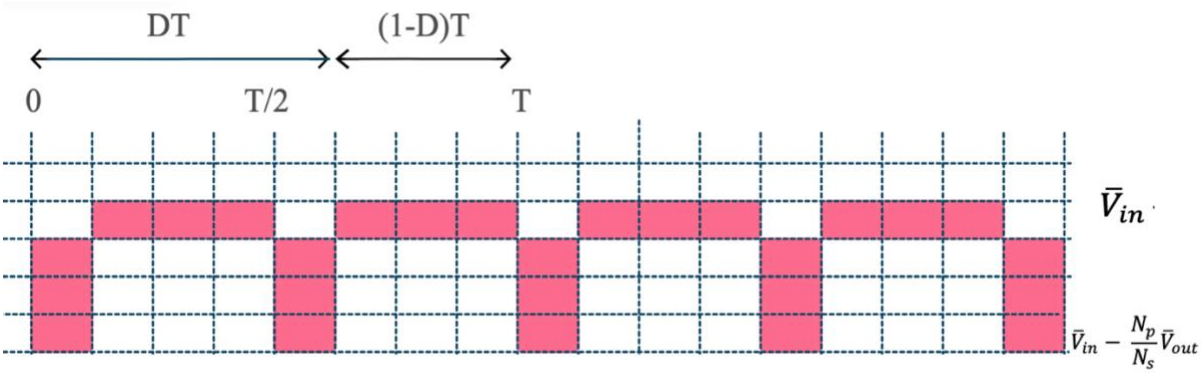

Figure 4-6. Inductor Voltage Waveform.

$$t_{on} = (1 - D)\, T \tag{4-5}$$

$$t_{off} = \frac{T}{2} - (1 - D)T = \frac{T}{2} - T + DT = \left(-\frac{1}{2} + D\right)T = -\left(\frac{1}{2} - D\right)T \tag{4-6}$$

After determining the expressions for t_{on} and t_{off}, the volt second balance of an ideal inductor can be applied. This rule determines that in steady state condition, the average or DC voltage across an ideal inductor is zero. The average power absorbed by an ideal inductor for steady state periodic operation is also determined to be zero. This is then used to derive the transfer function of the converter as shown in the analysis below.

Volt Second Balance Analysis:

$$V_{L_{on}} t_{on} + V_{L_{off}} t_{off} = 0$$

$$\left(\bar{V}_{in} - \frac{N_p}{N_s}\bar{V}_{out}\right)(1 - D)T - \bar{V}_{in}\left(\left(\frac{1}{2} - D\right)T\right) = 0$$

$$\bar{V}_{in} - \frac{N_p}{N_s}\bar{V}_{out} - \bar{V}_{in}D + \frac{N_p}{N_s}\bar{V}_{out}D - \bar{V}_{in}\frac{1}{2} + \bar{V}_{in}D = 0$$

$$\bar{V}_{in}\frac{1}{2} - \frac{N_p}{N_s}\bar{V}_{out} + \frac{N_p}{N_s}\bar{V}_{out}D = 0$$

$$\bar{V}_{in} - \frac{N_p}{N_s}\bar{V}_{out}(1-D) = 0 \tag{4-7}$$

Based on the results of the volt second balance analysis in equation 4-7, the voltage transfer function can be determined by rearranging the terms as shown in equation 4-8.

$$\bar{V}_{out} = \bar{V}_{in}\frac{N_s}{N_p}\frac{1}{2(1-D)} \tag{4-8}$$

To determine the current transfer function, one can use the assumption that the power into the converter (P_{in}) should be equivalent to the power that comes out of the converter (P_{out}) as this derivation uses all ideal components. This information, combined with the voltage transfer function can then be utilized to find the current transfer function.

$$\bar{P}_{in} = \bar{P}_{out} \rightarrow \bar{V}_{in}\bar{I}_{in} = \bar{V}_{out}\bar{I}_{out} \tag{4-9}$$

$$\bar{V}_{in} = \frac{P_{out}}{\bar{I}_{in}} = \frac{\bar{V}_{out}\bar{I}_{out}}{\bar{I}_{in}}$$

$$\bar{V}_{out} = \frac{\bar{V}_{out}\bar{I}_{out}}{\bar{I}_{in}}\frac{N_s}{N_p}\frac{1}{2(1-D)}$$

$$\bar{I}_{in} = \bar{I}_{out}\frac{N_s}{N_p}\frac{1}{2(1-D)}$$

$$\frac{\bar{I}_{out}}{\bar{I}_{in}} = 2\frac{N_p}{N_s}(1-D) \tag{4-10}$$

One factor of importance when designing the current-source DC-DC converter is to minimize the average input current as this input current represents the amount of current that is supplied by the land-based power supply. This land-based power supply

will be located several miles away from the submarine repeaters in which these converters will be deployed in. Input current affects the system in several ways as it impacts the rating, size and cost of the components utilized in the proposed converter. Since the primary side switches and transformer windings are in the series path of the input current, the current rating necessary for these components is directly proportional to the amount of input current. The amount of input current also impacts other aspects of the overall system such cable sizes, resistive losses, and the required rating and costs protection devices such as fuses and circuit breakers within the system. Utilizing equation 4-10 and the relationship that $\bar{I}_{out} = \frac{\bar{P}_{out}}{\bar{V}_{out}}$, a more detailed expression for input current can be determined, shown in equation 4-11.

$$\bar{I}_{in} = \frac{\bar{P}_{out}}{\bar{V}_{out}} \frac{N_s}{N_p} \frac{1}{2(1-D)} \tag{4-11}$$

Based on the current transfer function found in equation 4-10, an expression for the required duty cycle for the converter can be determined, as shown in equation 4-11. As mentioned previously, the duty cycle of the current-source DC-DC converter must be greater than 0.5 and less than 1. Due to this requirement, equation 4-12 can be used to find the relationship between the turns-ratio of the transformer and both the input and output current of the converter as shown in equation 4-13 to ensure that the above equation defines the minimum value for the turns ratio to ensure that the duty cycle is larger than 0.5.

$$D = 1 - \frac{1}{2} \frac{\bar{I}_{out}}{\bar{I}_{in}} \frac{N_s}{N_p} = 1 - \frac{1}{2} \frac{\bar{P}_{out}}{\bar{I}_{in} \bar{V}_{out}} \frac{N_s}{N_p} \tag{4-12}$$

$$\frac{1}{2}\frac{\bar{P}_{out}}{\bar{I}_{in}\bar{V}_{out}}\frac{N_s}{N_p} < 0.5 \quad \rightarrow \quad \bar{P}_{out} < \bar{I}_{in}\bar{V}_{out}\frac{N_p}{N_s} \quad \rightarrow \quad \bar{I}_{out}\bar{V}_{out} < \bar{I}_{in}\bar{V}_{out}\frac{N_p}{N_s}$$

$$\frac{N_p}{N_s} > \frac{\bar{I}_{out}}{\bar{I}_{in}} \tag{4-13}$$

Utilizing the equations derived above, an expression for the required duty cycle of the converter can be calculated. Given that the desired input current is 0.9 A, and the required output voltage is 24 V at 15 W, $\bar{I}_{out}$ can be calculated as:

$$\bar{I}_{out} = \frac{P_{out}}{\bar{V}_{out}} = \frac{15\ W}{24\ V} = 0.625\ A$$

After choosing a desired duty cycle between 0.5 and 1, the turns-ratio required for the converter can be calculated with the expression shown below:

$$D = 1 - \frac{1}{2}\left(\frac{0.625A}{0.9\ A}\right)\frac{N_s}{N_p} = 1 - 0.34722\frac{N_s}{N_p}$$

Expressions for both the minimum and maximum duty cycle for the design are based upon the requirements of the system as well as turns-ratio that has been chosen and can be seen below.

$$D_{min} = 1 - \frac{\bar{P}_{out_{max}}}{2\bar{I}_{in_{max}}\bar{V}_{out_{max}}\left(\frac{N_p}{N_s}\right)_{max}} \tag{4-14}$$

$$D_{max} = 1 - \frac{\bar{P}_{out_{min}}}{2\bar{I}_{in_{min}}\bar{V}_{out_{min}}\left(\frac{N_p}{N_s}\right)_{min}} \tag{4-15}$$

4.2 Relationship between Duty Cycle, Turns Ratio, and Input Current

Since several equations and relationships between the duty cycle, turns ratio and input current have been investigated, calculations can be made to determine which duty cycle can be utilized within the design. based upon the turns ratio chosen.

Table 4-1. Current Source DC-DC Converter Requirements

Current Source DC-DC Converter Requirements				
	Value	**Tolerance (%)**	**Maximum**	**Minimum**
Output Voltage (V)	24	2	24.48	23.52
Input Current (A)	0.9	5	0.945	0.86
Output Current (A)	0.625	5	0.656	0.593
Iout/Iin	0.694	-	-	-

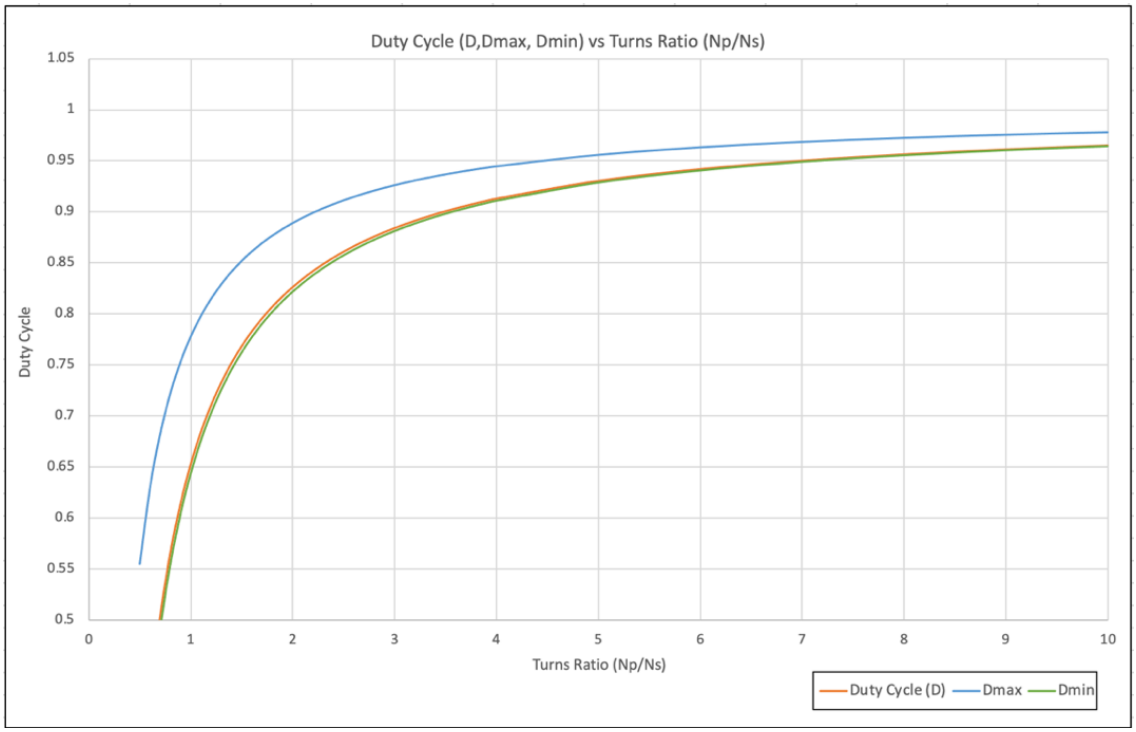

Figure 4-7. Duty Cycle vs Turns Ratio Graph.

Table 4-2. Duty, Maximum Duty, and Minimum Duty Cycles vs. Turns Ratio.

Duty Cycle vs Turns Ratio Calculation				
Turns Ratio (Np/Ns)	**Duty Cycle**	**(Np/Ns) > (Iout/Iin)?**	**Duty Cycle Maximum**	**Duty Cycle Minimum**
0.4	0.132	NO	0.444	0.108
0.5	0.306	NO	0.555	0.287
0.6	0.421	NO	0.629	0.406
0.7	0.504	YES	0.682	0.491
0.8	0.566	YES	0.722	0.554
0.9	0.614	YES	0.753	0.604
1	0.653	YES	0.778	0.643
1.1	0.684	YES	0.798	0.676
1.2	0.711	YES	0.815	0.703
1.3	0.733	YES	0.829	0.726
1.4	0.752	YES	0.841	0.745
1.5	0.769	YES	0.852	0.762
1.6	0.783	YES	0.861	0.777
1.7	0.796	YES	0.869	0.790
1.8	0.807	YES	0.876	0.802
1.9	0.817	YES	0.883	0.812
2	0.826	YES	0.889	0.822
2.1	0.835	YES	0.894	0.830
2.2	0.842	YES	0.899	0.838
2.3	0.849	YES	0.903	0.845
2.4	0.855	YES	0.907	0.851
2.5	0.861	YES	0.911	0.857
2.6	0.866	YES	0.914	0.863
2.7	0.871	YES	0.918	0.868
2.8	0.876	YES	0.921	0.873
2.9	0.880	YES	0.923	0.877

3	0.884	YES	0.926	0.881
3.1	0.888	YES	0.928	0.885
3.2	0.891	YES	0.930	0.889
3.3	0.895	YES	0.933	0.892
3.4	0.898	YES	0.935	0.895
3.5	0.901	YES	0.936	0.898
3.6	0.904	YES	0.938	0.901
3.7	0.906	YES	0.940	0.904
3.8	0.909	YES	0.941	0.906
3.9	0.911	YES	0.943	0.909
4	0.913	YES	0.944	0.911
5	0.931	YES	0.956	0.929
6	0.942	YES	0.963	0.941
7	0.950	YES	0.968	0.949
8	0.957	YES	0.972	0.955
9	0.961	YES	0.975	0.960
10	0.965	YES	0.978	0.964

Figure 4.7 shows that the results for the minimum duty cycle are similar to the standard duty cycle, with an average difference of around 0.005 between each value. The maximum duty cycle for each turns-ratio was calculated to be significantly higher in comparison to the standard duty cycle, with an average difference of 0.09 between each point from the turns-ratio range of 0.5-4. It can also be seen that as the turns-ratio increases, the three data sets begin to converge to a duty cycle value close to 1.

Based on the data above, one now has a range of values to choose a turns-ratio from, with a turns ratio of 2 being chosen for this specific converter design. With the turns ratio being chosen, the duty cycle to be utilized in the design was calculated to be

0.826 and the values of D_{min} and D_{max} for the converter are 0.821 and 0.888, respectively.

Furthermore, a necessary step for designing the current-source DC-DC converter is to determine each component's ratings. These ratings will be calculated using the given design requirements of the system as well as steady state analysis of the current-source DC-DC converter. These derivations and ratings are based upon ideal components. Non-linear effects, parasitic resistance, inductance, or capacitance will not be considered in these derivations.

4.3 Switch Rating Calculations

The voltage and current ratings of the switches used in the proposed converter are the two primary characteristics one must use when initially selecting a switch. Other characteristics such as operating frequency, losses, and driving requirements are looked at as secondary criteria, when selecting components. To determine what this rating is, one can perform analysis of the circuit in steady state 1, as shown in Figure 4-3 previously. In the first state, switches S_1 and S_2 are on while switches S_3 and S_4 are off. As a result, diodes D_1 and D_2 conduct which causes the output voltage $\bar{V}_{out}$ to appear across the secondary winding of the transformer. This means that the voltage on the secondary side of the transformer (V_S) is now equivalent to $\bar{V}_{out}$. Then, a reflected voltage is produced across the primary winding (V_P) as shown in equation 4-16.

$$V_S = \bar{V}_{out}$$
$$V_P = \frac{N_p}{N_s} V_S = \frac{N_p}{N_s} \bar{V}_{out} \tag{4-16}$$

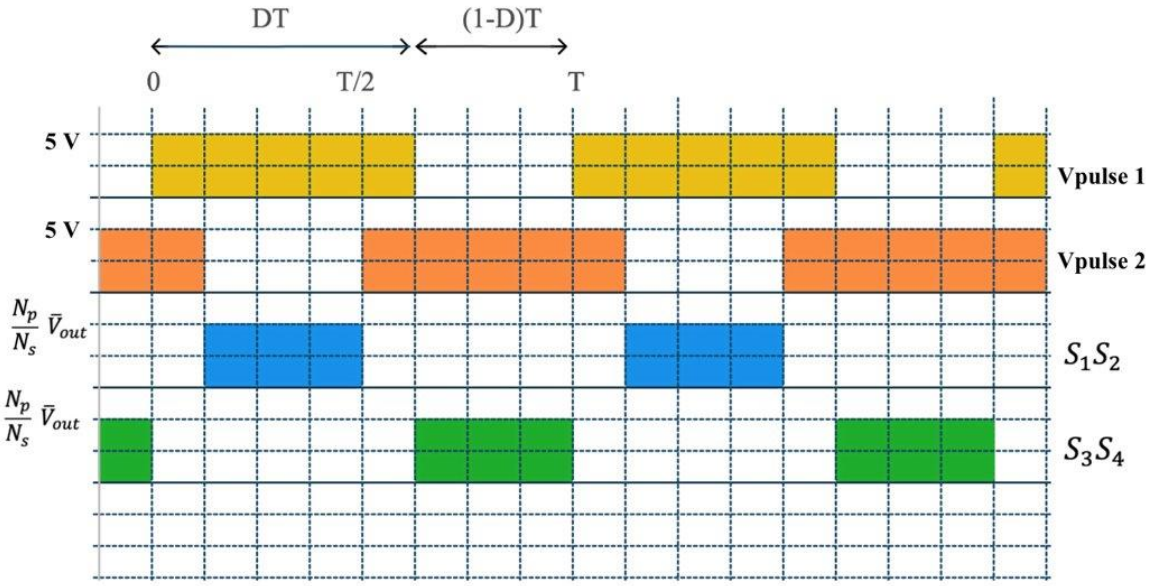

Figure 4-8. Primary Side Switching Voltage Waveform.

Based on the Kirchhoff's voltage law, the reflected voltage V_P, becomes the new voltage rating for switches S_1 and S_2. A similar analysis can be done on the circuit in steady state 2 in which switches S_1 and S_2 are off while switches S_3 and S_4 are on. Due to the symmetry of the design, switches S_3 and S_4 end up having the same voltage ratings as determined for switches S_1 and S_2 previously. The summary of the voltage rating for the 4 switches utilized within the design as seen in the expression shown in equation 4-17. To find the current rating of the switches, the first step is to look at the amount of current going through each switch, as shown in Figure 4-8. Based upon this expression and a turns ratio of 2, the voltage rating for each switch in the design is approximately 48 V.

$$V_{SW1} = V_{SW2} = V_{SW3} = V_{SW4} = \frac{N_p}{N_s}\bar{V}_{out} \tag{4-17}$$

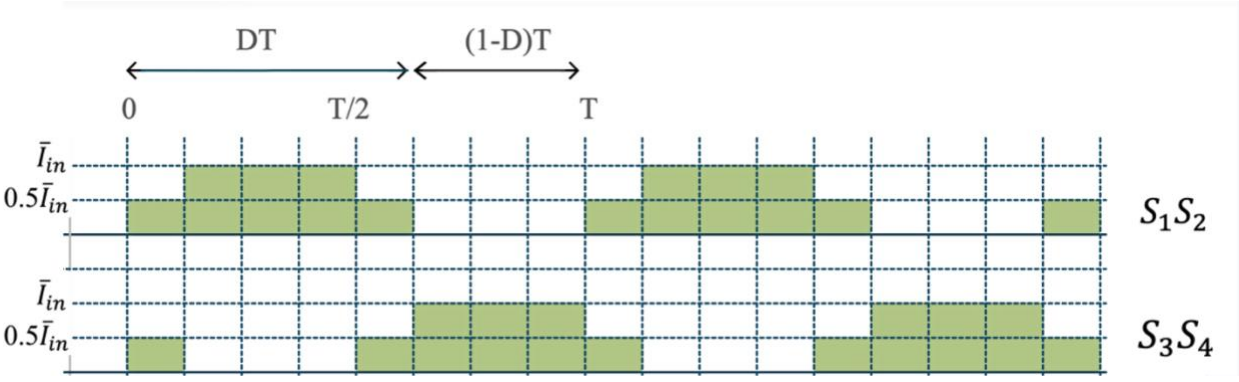

Figure 4-9. Primary Side Switching Current Waveform.

Figure 4-8 shows that when a switching pair is conducting on the primary side while the other pair is off, the full input current $0.5\bar{I}_{in}$ can flow through the conducting pair of switches. However, when all 4 switches are conducting, each switch would share the input current equally. These expressions can be seen in equations 4-18 and 4-19 respectively.

$$\bar{I}_{SW_{t1}} = \bar{I}_{in} \tag{4-18}$$

$$\bar{I}_{SW_{t2}} = \frac{\bar{I}_{in}}{2} \tag{4-19}$$

Using the results from equations 4-18 and 4-19, as well as the switching waveform, the average current passing through each switch can be derived. This value can then be used as a baseline for choosing which switches to utilize in the design. For the input current of 0.9A, $\bar{I}_{SW}$ is calculated to be 0.45A.

$$\bar{I}_{SW} = \frac{Area\ Under\ Switch\ Current\ Waveform}{Period}$$

$$\bar{I}_{SW} = \frac{\bar{I}_{in}\,(1-D)T}{T} + 2\,\frac{\left(\frac{\bar{I}_{in}}{2}\right)\left(\frac{DT-(1-D)T}{2}\right)}{T}$$

$$\bar{I}_{SW} = \bar{I}_{in}(1-D) + \bar{I}_{in}\left(D - \frac{1}{2}\right)$$

$$\bar{I}_{SW} = \bar{I}_{in}\left[(1-D) + \left(D - \tfrac{1}{2}\right)\right] = \bar{I}_{in}\tfrac{1}{2}$$

$$\bar{I}_{SW} = \bar{I}_{SW1} = \bar{I}_{SW2} = \bar{I}_{SW3} = \bar{I}_{SW4} = \bar{I}_{in}\tfrac{1}{2} \tag{4-20}$$

4.4 Rectifier Diode Rating Calculations

Like the switch voltage rating calculations, the diode voltage rating is based upon its steady-state maximum value which is the primary characteristics one must use when initially selecting a diode. Since the proposed converter will be operating at a switching frequency of 250 kHz and it has an output voltage below 100 V, the diode type choice will be between a Schottky or SBR type. To determine what this rating is, one can perform analysis of the circuit in steady state 1, as shown in Figure 4-3 previously. In the first state, switches S_1 and S_2 are on while switches S_3 and S_4 are off. As a result, diodes D_1 and D_2 conduct and see a voltage equivalent to $\bar{V}_{out}$. This means that each diode must have a voltage rating that can handle the amount of output voltage from the converter. When the same analysis is performed in steady state 2, it is found that diodes D_3 and D_4 conduct and see a voltage equivalent to $\bar{V}_{out}$ as well. This indicates that all diodes chosen for the current-source DC-DC converter must be able to handle this amount of voltage. The summary of the voltage rating for the four diodes utilized within the design is given in equation 4-21.

$$V_{D1} = V_{D2} = V_{D3} = V_{D4} = \bar{V}_{out} \tag{4-21}$$

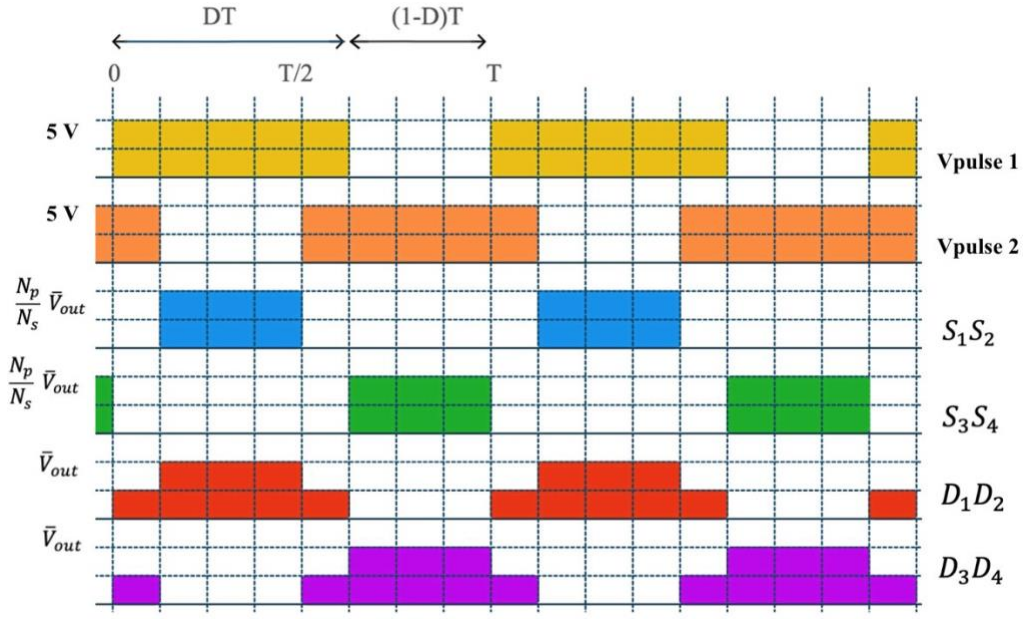

Figure 4-10. Diode and Switching Voltage Waveforms

In the case of the proposed converter, the voltage ratings of the diodes must be 24 V. To find the current rating of the diodes, one must analyze the diode current waveforms alongside the switching current waveforms, as shown in Figure 4-9.

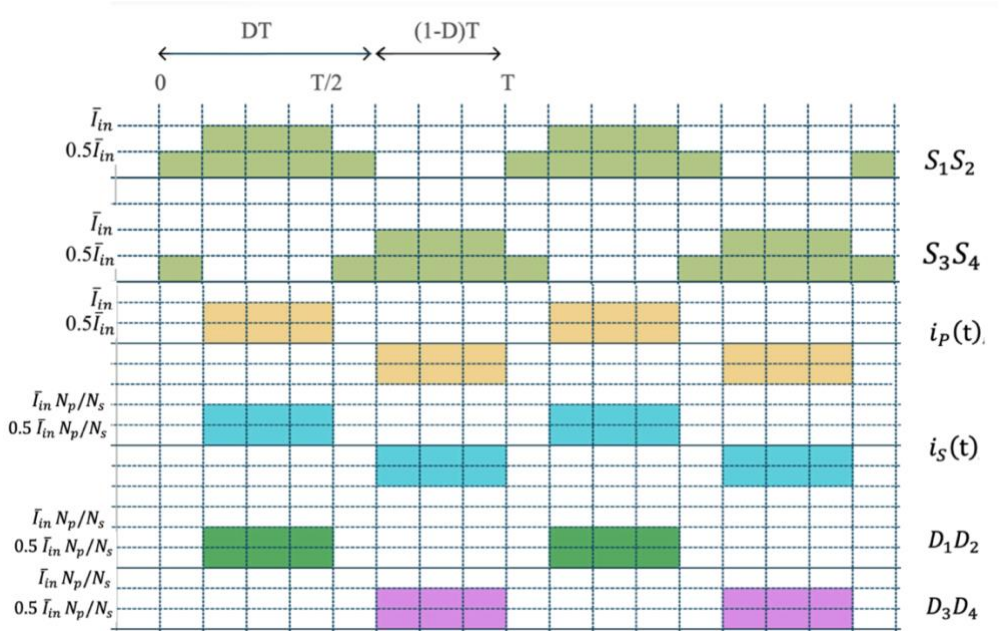

Figure 4-11. Diode and Switching Current Waveforms

When one of the two switching pairs, S_1 and S_2 or S_3 and S_4, are conducting on the primary side, current flows through the diode pair of D_1 and D_2 or D_3 and D_4 on the secondary side. This current is equivalent to the current from the primary side that is then reflected onto the secondary side, whose equation is shown in equation 4-22.

$$\bar{I}_{SW_{peak}} = \bar{I}_{in} \frac{N_p}{N_s} \tag{4-22}$$

In the case that all four switches are conducting on the primary side, there will be no current flow through the diodes as it behaves as a short circuit. With this knowledge, the average current through each diode can be determined and this value can be utilized when choosing a rectifier diode. The equation for this value can be seen in equation 4-23.

$$\bar{I}_D = \frac{Area\ Under\ Diode\ Current\ Waveform}{Period}$$

$$\bar{I}_D = \frac{\bar{I}_{in} \frac{N_p}{N_s} (1 - D)T}{T}$$

$$\bar{I}_D = \bar{I}_{D1} = \bar{I}_{D2} = \bar{I}_{D3} = \bar{I}_{D4} = \bar{I}_{in} \frac{N_p}{N_s} (1 - D) \tag{4-23}$$

Based on the duty cycle and turns ratio chosen previously for the converter, the average current was calculated to be 0.3132 A, while the peak switch current was calculated to be 1.8 A.

4.5 Output Capacitor Ratings

To suppress any fluctuations of output voltage in the converter, an output capacitor can be added onto the secondary side of the converter. Furthermore, the capacitor can also act as a source of energy when all switches on the primary side are

conducting and there is no supply of current. Figure 4-10 shows how the secondary side of the converter would be altered with the addition of the output capacitor C_1.

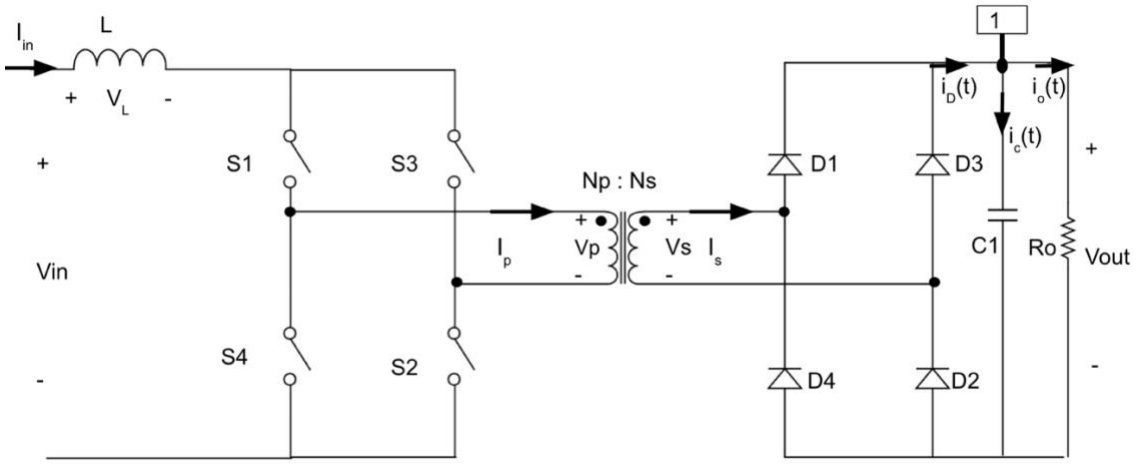

Figure 4-12 Proposed Current-Source DC-DC Converter with Added Output Capacitor

By utilizing Kirchhoff's current law at node 1 labeled above, an expression can be formed for the rectifier output current i_D(t) where $i_D(\mathrm{t}) = i_C(\mathrm{t}) + i_{out}(\mathrm{t})$. This equation using average values of each current can be seen below in equation 4-24.

$$\bar{I}_D = \bar{I}_C + \bar{I}_{out} \tag{4-24}$$

Based upon the rule of Amps Second Balance of an ideal capacitor which states that in steady state periodic operation, the average current through an ideal capacitor is equal to zero, the expression in equation 4-24 reduces to the expression in equation 4-25.

$$\bar{I}_D = \bar{I}_{out} \tag{4-25}$$

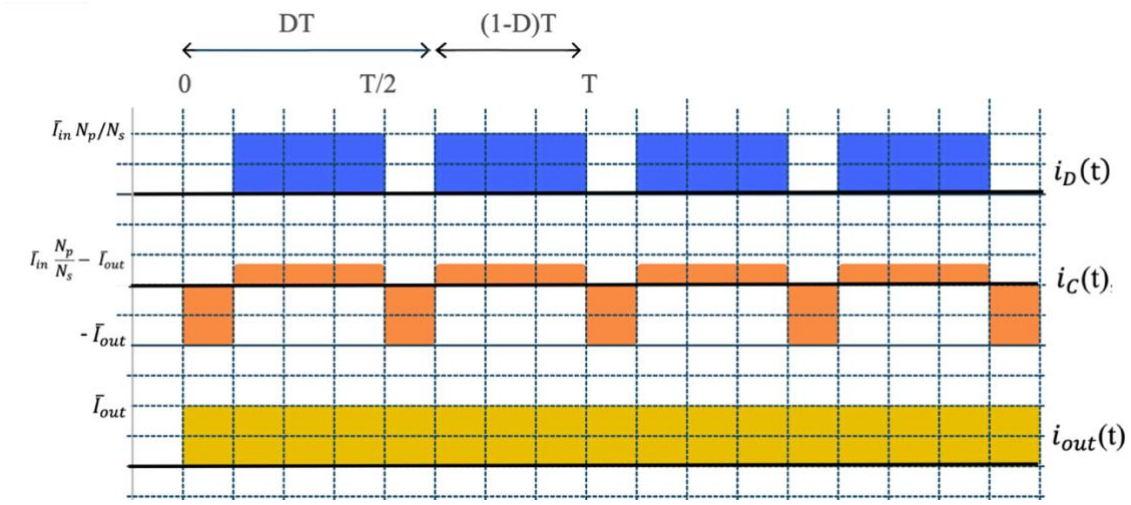

Figure 4-13. $i_D(t)$, $i_C(t)$, and $i_{out}(t)$ Current Waveforms.

As a result, the output capacitor current will be the same as that of the rectifier current waveform shifted down by $\bar{I}_{out}$. Knowing this current, an expression for the critical capacitance can be found. This expression utilizes the charge equation which states that the charge of a capacitor is equal to the product of the output capacitance (C_1) and the output voltage peak to peak ripple (ΔV_o). This equation can be used to describe an area of positive or negative charge and can be seen in equation 4-26. By utilizing the capacitor current waveform, an expression for the area of positive charge can be determined as well as shown in equation 4-27.

$$q = C_1 \Delta V_o \tag{4-26}$$

$$q = \left(\bar{I}_{in} \frac{N_p}{N_s} - \bar{I}_{out} \right)(1 - D)T \tag{4-27}$$

By equating these two expressions, a value for the output capacitance can be determined in terms of frequency instead of period as shown in equation 4-28.

$$\left(\bar{I}_{in} \frac{N_p}{N_s} - \bar{I}_{out} \right)(1-D)T = C_1 \Delta V_o$$

$$C_1 = \left(\bar{I}_{in} \frac{N_p}{N_s} - \bar{I}_{out} \right)(1-D)T \frac{1}{\Delta V_o}$$

$$C_1 = \left(\bar{I}_{in} \frac{N_p}{N_s} - \bar{I}_{out} \right)(1-D)T \frac{1}{\Delta V_o} = \left(\bar{I}_{in} \frac{N_p}{N_s} - \bar{I}_{out} \right)\frac{(1-D)}{\Delta V_o f} \quad (4\text{-}28)$$

In the case of the proposed converter design, the chosen switching frequency is 250 kHz. Based on the assumption that the output voltage ripple is 0.1 V, an output capacitance of around 8 µF is calculated. This value can then be rounded up to the standard value of 10 µF, which can be utilized within the design.

Another parameter needed for sizing the output capacitor is its RMS current. This is an important calculation as non-ideal real capacitors often have some internal equivalent series resistance, otherwise known as ESR. The RMS current that flows through the ESR will produce a loss in power equivalent to the expression found in equation 4-29.

$$P_{C1} = i_{C1_{RMS}}^2 ESR \quad (4\text{-}29)$$

For the proposed converter, the RMS current through the output capacitor may be calculated from the output capacitor current waveform shown in Figure 4-11 .

$$I_{crms} = \sqrt{\frac{1}{T}\left(\int_0^{t_1} I_{out}^2 \, dt + \int_{t_1}^{t_2} \left(\bar{I}_{in} \frac{N_p}{N_s} - \bar{I}_{out} \right)^2 \right)}$$

$$I_{crms} = \sqrt{\frac{1}{T}\left(I_{out}^2 \, t_1 + \left(\bar{I}_{in} \frac{N_p}{N_s} - \bar{I}_{out} \right)^2 \right)(t_1 - t_2)}$$

$$I_{crms} = \sqrt{\frac{1}{T}\left(I_{out}^2\left(\frac{T}{2} - (1-D)T\right) + \left(\bar{I}_{in}\frac{N_p}{N_s} - \bar{I}_{out}\right)^2\right)(1-D)T}$$

$$I_{crms} = \sqrt{\left(I_{out}^2\left(D - \frac{1}{2}\right) + \left(\bar{I}_{in}\frac{N_p}{N_s} - \bar{I}_{out}\right)^2\right)(1-D)}$$

$$I_{crms} = \sqrt{\frac{1}{2}I_{out}^2 + \left(\bar{I}_{in}\frac{N_p}{N_s}\right)^2(1-D) - 2\bar{I}_{in}\bar{I}_{out}\frac{N_p}{N_s}(1-D)} \quad (4\text{-}30)$$

Based upon the equation derived in 4-30, the value of I_{crms} was calculated to be 0.606 A.

When determining the voltage rating of the output capacitor, it is known that output capacitor is in parallel with the output resistor. This means that the capacitor should be rated for the average output voltage of the converter alongside any additional voltage ripple present in the converter. The expression for voltage rating can be shown in equation 4-31.

$$V_{C1_{max}} = \bar{V}_{out} + \frac{\Delta V_o}{2} \quad (4\text{-}31)$$

Chapter 5
SIMULATION RESULTS AND ANALYSIS

Chapter 5 will discuss the development of a simulation model for the proposed converter, demonstrating both the functionality and operation of the design. Simulations will be performed using LTspice, a high-performance SPICE simulator software developed by Analog Devices which includes a graphical schematic capture interface [13]. This software was selected as it is accessible, user-friendly, and contains an extensive library of real-world circuit components, allowing one to thoroughly analyze a circuit design.

5.1 Simulation Utilizing Ideal Components

To verify the results of the analysis presented in chapter 4 and display the functionality of the Current-Source DC-DC converter, an initial computer simulation of the proposed design was constructed utilizing both ideal and close to ideal components as well as the parameters determined from the system requirements. To ensure a turns ratio of 2:1 as chosen previously, a transformer with a primary winding inductance of 400µF and a secondary winding inductance of 100µF with a coupling coefficient of 1 was used. A switching frequency of 250 kHz was chosen for the converter, reflected by utilizing a period of 4µs within the simulation. Ideal switches, diodes, resistors, capacitors, voltage sources, and current sources were placed into the simulation to ensure that the results can closely match those derived previously. Furthermore, to maintain a regulated 24V output voltage, a closed loop output voltage monitoring divider resistor network, utilizing a type III compensator design was implemented within the design. In this type of design, the

output voltage of the circuit is fed back and compared to a stable reference voltage. Any difference between the two generates a compensating error voltage which tends to move the output voltage towards the design specification. This type of compensator is used to provide enough phase margin to keep the loop stable within certain applications. The addition of the type III compensator also helps with any existing ESR on the capacitor, causing a steep roll off after the capacitor's ESR frequency.

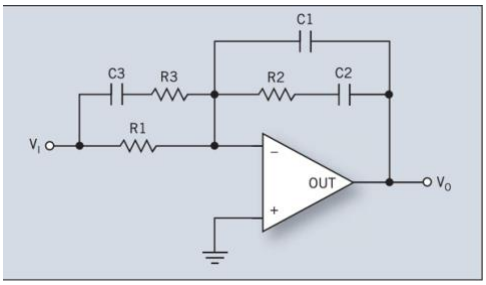

Figure 5-1. Circuit Diagram of Standard Type III Compensator [14]

The transfer function of this compensator in the s-domain can be seen in equation 5-1. Based on the needs and application of a circuit, resistor and capacitor values can be chosen for the desired pole and zero frequencies, gain, and phase margins.

$$\frac{V_{out}}{V_{in}} = \frac{(sC_2R_2 + 1)(sC_3(R_1 + R_3) + 1)}{R_1(C_1 + C_2)s(s\left(\frac{C_1C_2}{C_1 + C_2}\right)R_2 + 1)(sC_3R_3 + 1)}$$

$$\frac{V_{out}}{V_{in}} = \frac{s^2C_2C_3R_2(R_1 + R_3) + s\left(C_2R_2 + C_3(R_1 + R_3)\right) + 1}{s^3C_1C_2C_3R_1R_2R_3 + s^2R_1(C_1C_2R_2 + (C_1 + C_2)C_3R_3 + sR_1(C_1 + C_2)} \quad (5\text{-}1)$$

The current-source DC-DC converter simulation also utilizes the LT1721 chip, which is a high-speed quad comparator optimized for single supply operation [15]. The output of the LT1721 is utilized as a voltage input into the switches to ensure accurate switching frequency and as a part of the voltage monitoring network. One of the benefits to using

the LT1721 within the design is that the pinouts of the LT1721 have been arranged to minimize problems by placing the most sensitive inputs away from the outputs, shielded by the power rails [15]. Figure 5-2 shows the schematic of the proposed converter with ideal components and Table 5-1 shows LTSpice Parameters utilized within the design

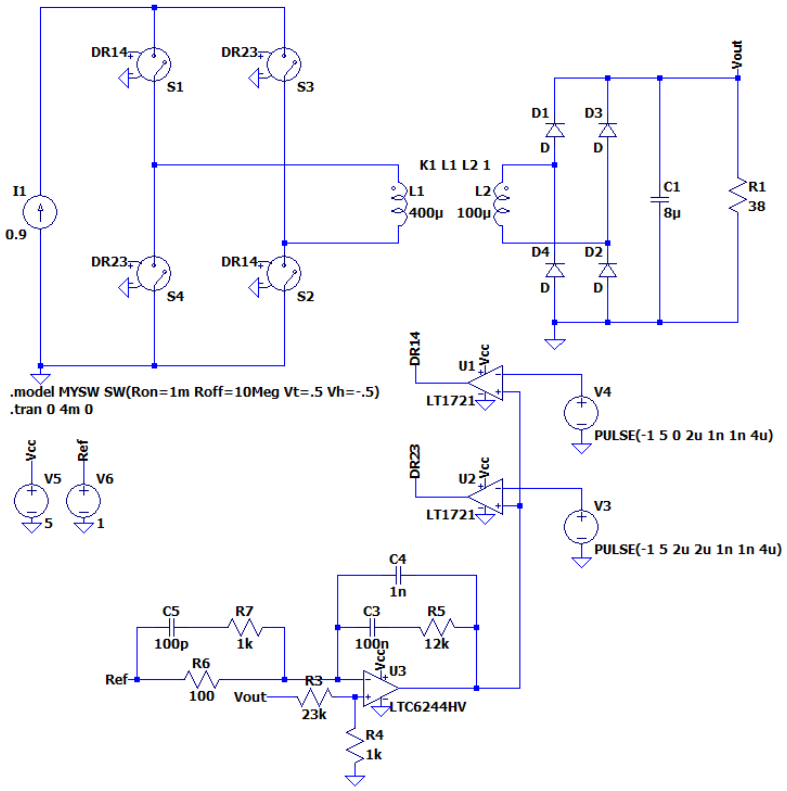

Figure 5-2. LTSpice Schematic of Proposed Converter with Ideal Components

Table 5-1. Parameters Utilized in LTSpice Simulation

Parameter	Value
Input Current	0.9 A
Output Current	0.625 A
Output Voltage	24 V
Output Power	15 W
Switching Frequency	250 KHz
Transformer Turns Ratio	2
Duty Cycle	0.826

After the LTSpice schematic was created, it was then simulated and analyzed to determine if the waveforms matched expected results.

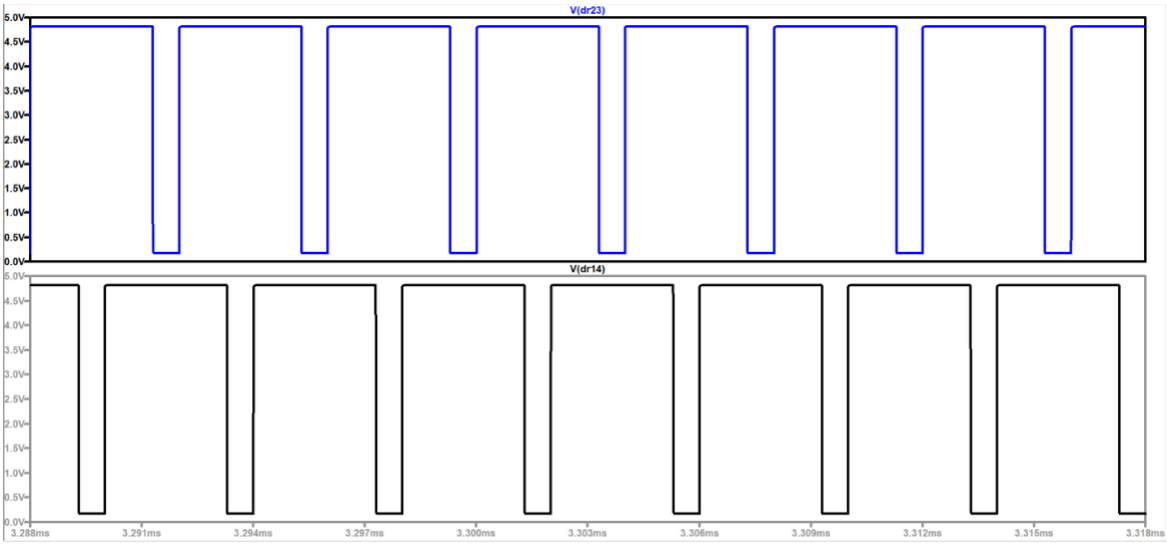

Figure 5-3: Switching Pulses used to Verify a Duty Cycle of 0.826

As shown in Figure 5-3, the chosen duty cycle matches the chosen value of 0.826. These pulses are used as voltage inputs into the switches on the primary side of the converter.

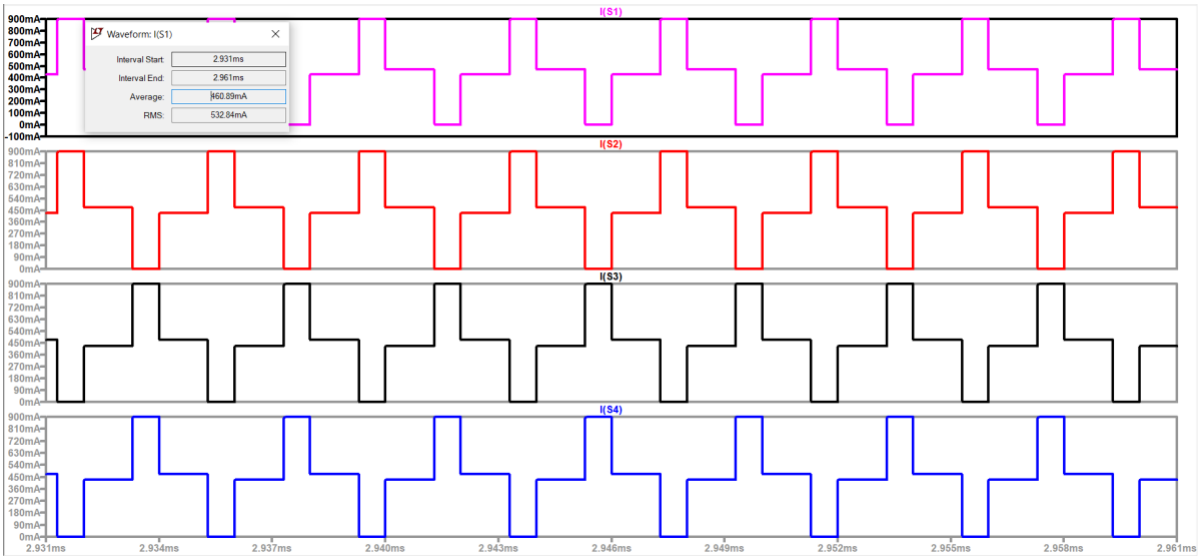

Figure 5-4. Switch Current Waveforms from Ideal Components Simulation

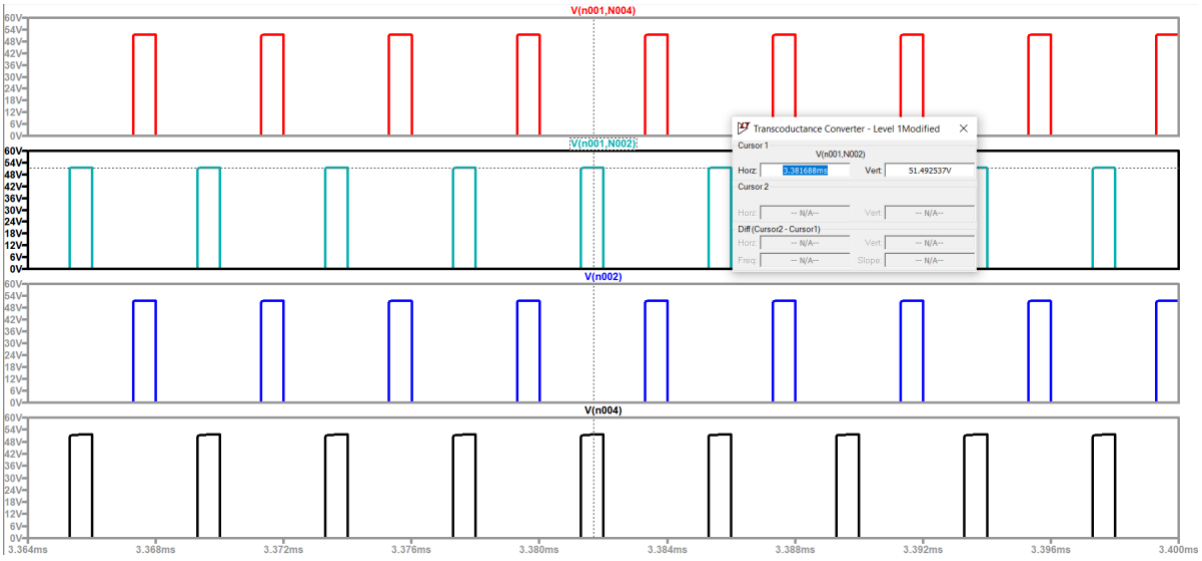

Figure 5-5. Switch Voltage Waveforms from Ideal Components Simulation

In Figure 5-4 it can be shown that the switch current waveform has the same general shape as expected, with a peak current of 0.9A, and an average current of 0.46A, which is 0.01A larger than the expected value of 0.45A. The figure also shows that switches S1 and S2 have the same waveforms, while switches S3 and S4 have the same waveforms. The peak switch voltage seen in Figure 5-5 was found to be 51.4V, which was 3.4V larger than the expected voltage of 48V. This difference has the most impact when choosing components for the converter as they should be rated to withstand both peak current and voltage values. Figure 5-6 demonstrates a summary of the switch waveforms, showing how duty cycle impacts the shape of both the current and voltage waveforms, allowing us to further verify the results.

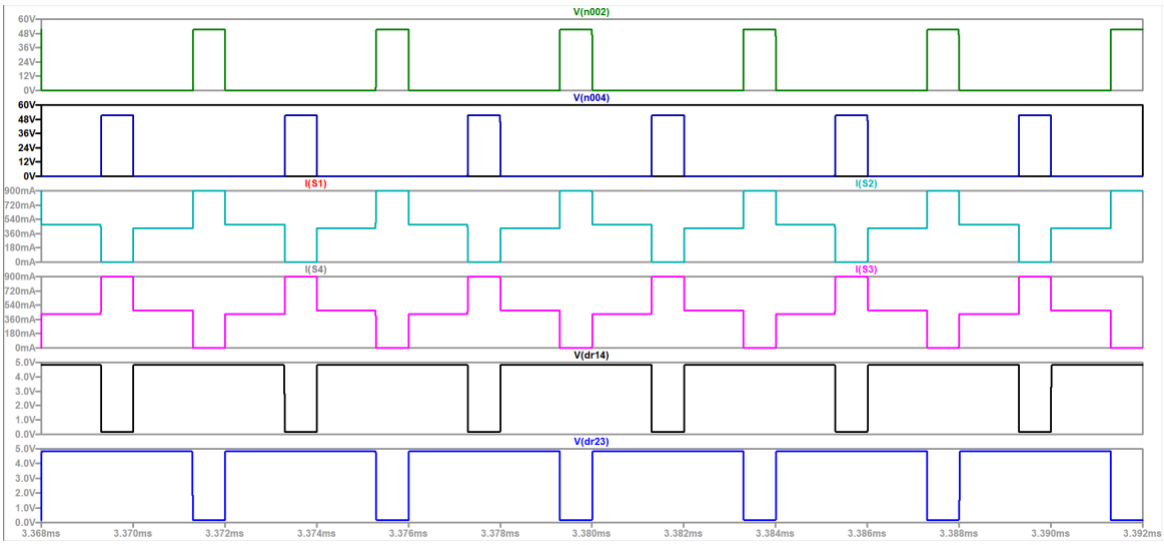

Figure 5-6. Summary of Switch Waveforms from Ideal Components Simulation

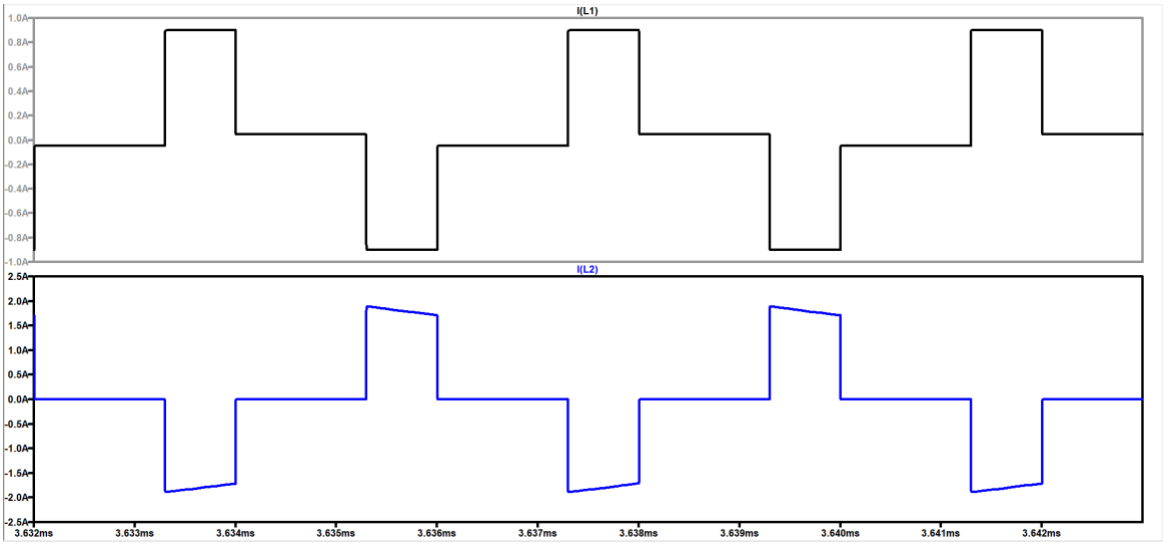

Figure 5-7. Primary and Secondary Inductor Currents from Ideal Components Simulation

Figure 5-7. shows the Primary and Secondary Inductor current, and from this data it can be seen that the average current on the primary side is 0.9 A while the secondary side of the waveform has a maximum current of 1.98 A, and an average value of 1.86 A, which is close to the expected value of 1.8A.

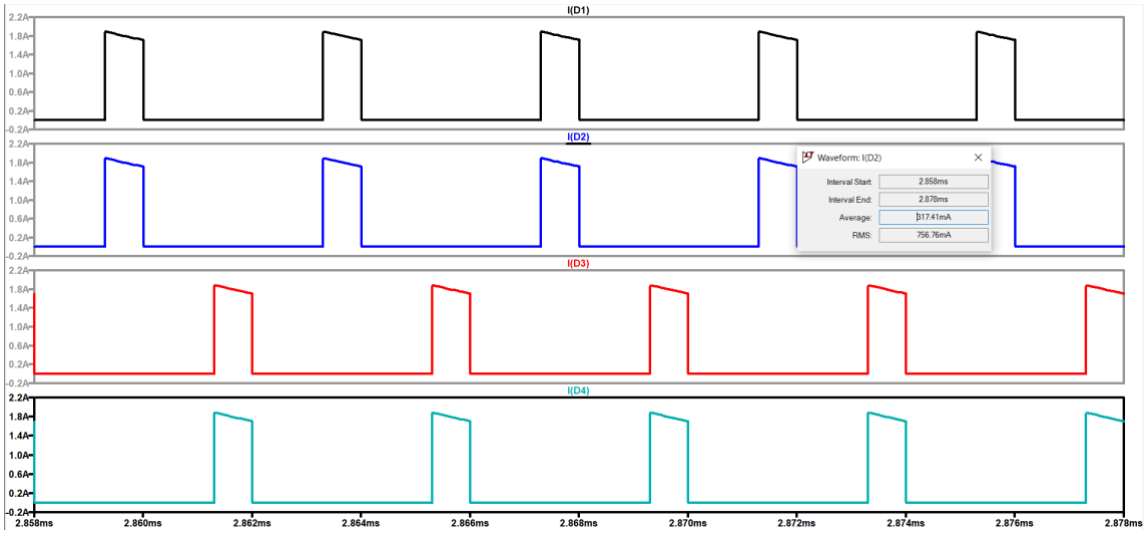

Figure 5-8. Diode Current Waveforms from Ideal Components Simulation

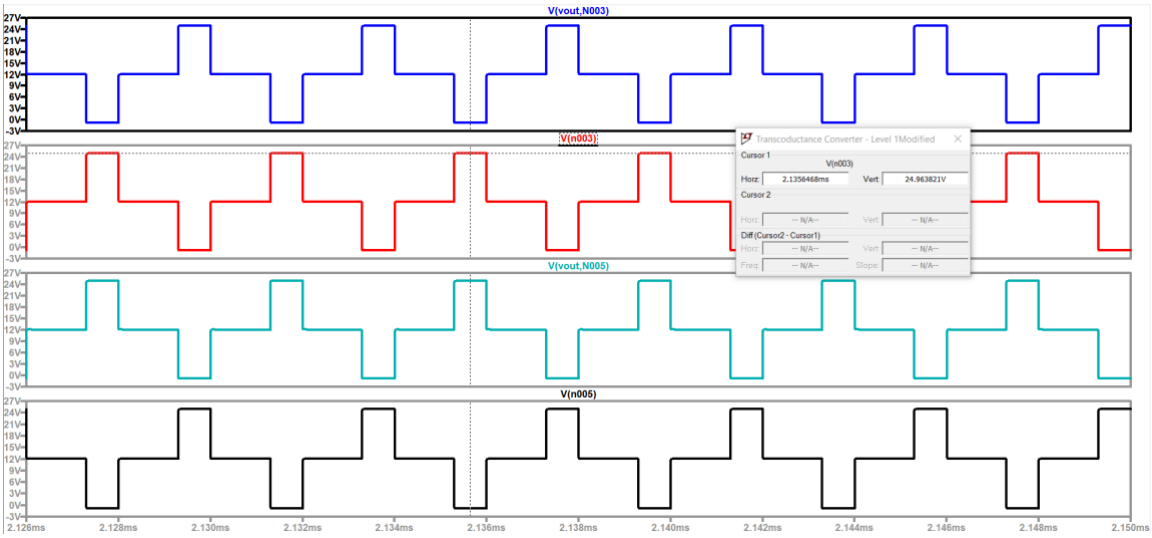

Figure 5-9. Diode Voltage Waveforms from Ideal Components Simulation

Figures 5-8 and 5-9 show the Diode Current and Voltage waveforms. It is shown that there is a peak current of 1.895A and an average current of 0.318A, which was 0.005A larger than the calculated value of 0.313A. The peak voltage through the diode was 24.9V, with an average voltage value of 12.08V. This value was 0.9V larger than the calculated value of 24V, however the overall results of these waveforms are similar to what was expected.

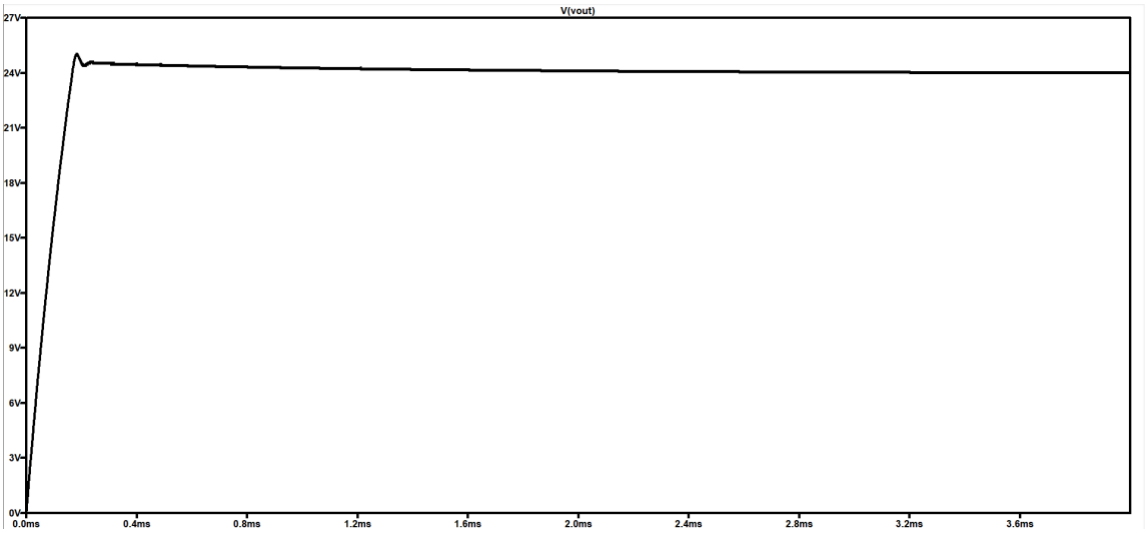

Figure 5-10. Output Voltage Waveform from Ideal Components Simulation

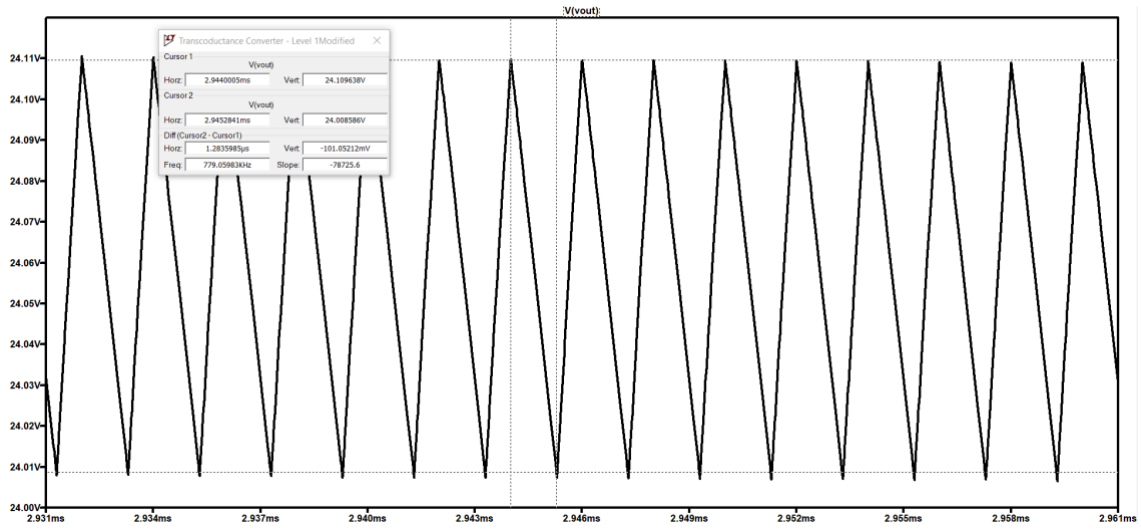

Figure 5-11. Output Voltage Peak to Peak Ripple from Ideal Components Simulation

The results from figures 5-10 and 5-11 show that $\bar{V}_{out}$ was measured to be 24.063V. The voltage peak to peak ripple (ΔV_o) was determined to be 0.101V, which matches with the expected value of 0.1V that comes with choosing an 8uF capacitor. This output voltage matches the requirements of the system as previously defined.

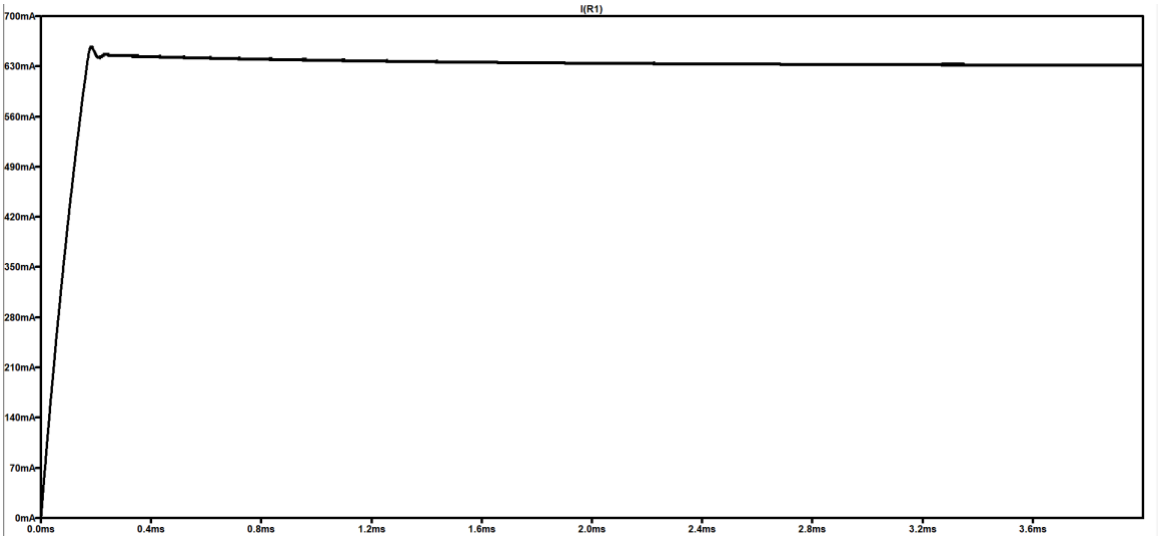

Figure 5-12. Output Current Waveform from Ideal Components Simulation

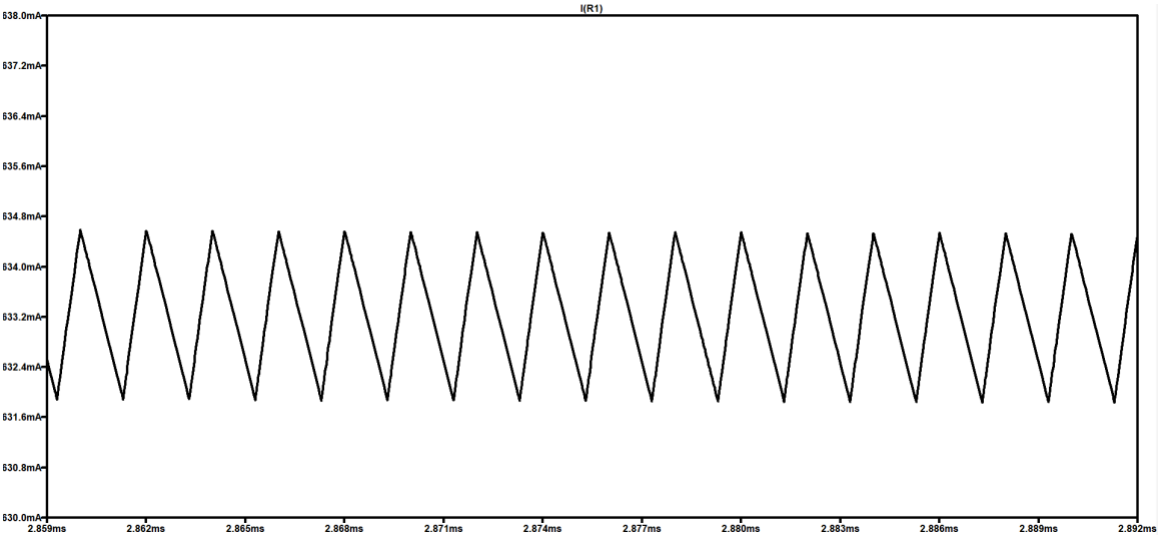

Figure 5-13. Output Current Peak to Peak Ripple from Ideal Components Simulation

Based on the results from Figures 5-12 and 5-13, it was determined that $\bar{I}_{out}$ was measured to be 0.634A, which is larger than the desired current of 0.625A by 0.009 A. It was also found that there was an output current ripple of 0.002A, which results in an 0.426% peak to peak output current ripple.

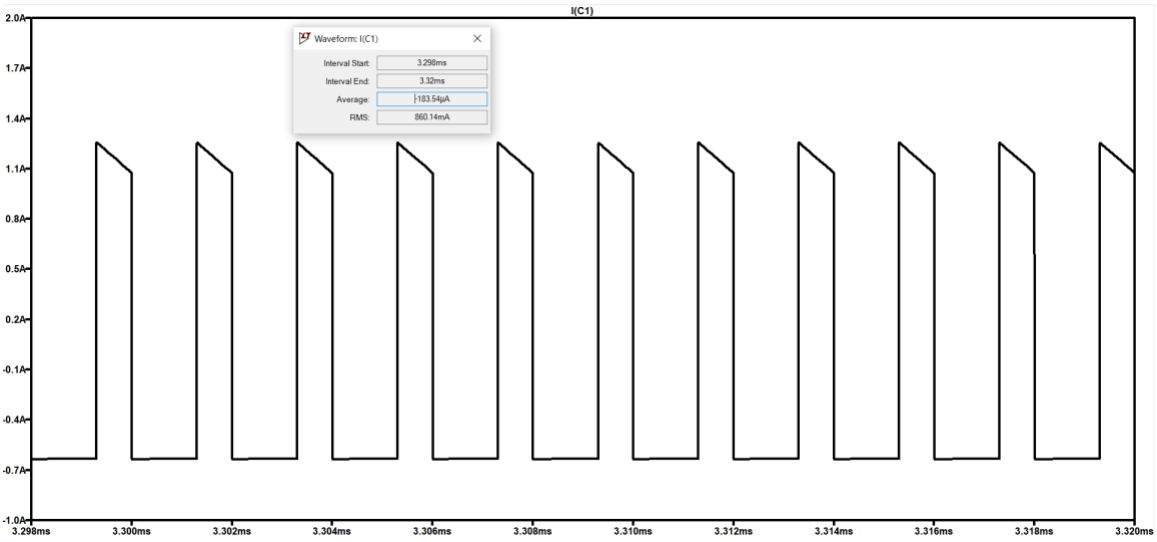

Figure 5-14. Output Capacitor Current Waveform from Ideal Components Simulation

An output capacitor of 8µF was utilized within the design. It was found that the peak current through the capacitor was 1.2A and the RMS current as 0.860A, which was larger than the calculated value of 0.606A. Some of these differences could be accounted for due to the difference in output current as the calculation for I_{crms} is dependent on output current. An increase in this current resulted in an increase in the capacitor RMS current. Despite this difference, the addition of the 8µF output capacitor impacted the output voltage ripple by close to 0.1V, which was expected based on the equation 4-28 shown previously. To change the value of the output voltage ripple, the value of the output capacitor can be modified for the desired results.

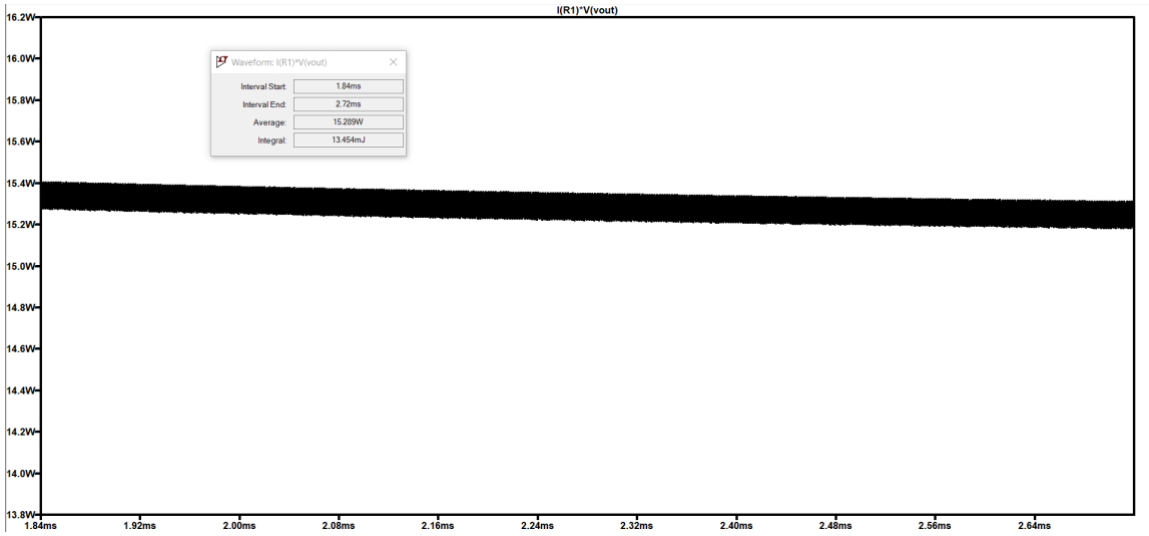

Figure 5-15. Output Power Waveform from Ideal Components Simulation

As shown in Figure 5-15, the output power was determined to be 15.289W, when the required output power was 15W, showing an increase of 0.289 W, which is slightly under a 2% tolerance. The average input power into the system was determined to be 16.35 W based upon the simulation results. By using these two values, the overall efficiency of the converter was calculated to be 93.5%. A summary of the results of this simulation in comparison to the previously calculated results can be found in Table 5-2.

Table 5-2. Comparison of Calculated vs Simulated Values

Parameter	Calculated Value	Simulated Value	% Difference
Average Switch Current	0.45 A	0.46 A	2.19 %
Peak Switch Voltage	48 V	51.4 V	6.84 %
Average Diode Current	0.313 A	0.318 A	1.58 %
Peak Diode Voltage	24 V	24.9 V	3.68 %
Average Output Current	0.625 A	0.634 A	1.429 %
Average Output Voltage	24 V	24.063 V	0.262 %
Average Output Power	15 W	15.289 W	1.908 %
I_{crms}	0.606 A	0.860 A	34.65 %
Output Voltage Ripple	0.1 V	0.101 V	0.99 %

Based on the values shown in the Table 5-2, it has been determined that the overall results of the simulations with ideal components closely matched the theoretical values determined previously, verifying the accuracy of the calculations and derivations previously made. The data that shows the largest percent difference is in the calculation of I_{crms} , which is highly dependent on the output current. Another significant difference is that of the peak switch voltage, which ideally was derived to be 48 volts, but in simulation was determined to be 51.4 volts. Since this difference did not end up impacting the overall performance of the design significantly, the switches should be rated for a voltage above 51.4 V when using real components.

5.2 Simulation Utilizing Real Components

In the second simulation developed, most of the ideal components were replaced with real models of components. The primary objective of this simulation is to show the feasibility in constructing the converter through commercially available components as well as verifying the functionality of the proposed converter design. Several small changes were made to the overall design as well to improve the performance of the converter and add protection to the circuit. One change included adding protection diodes at the input and the output to protect the circuit from potential reverse voltage and currents. An additional change was adding an RC branch across the primary winding to suppress any high frequency ringing and protect the device from any potential high voltage stress. Furthermore, some of the differences that were seen in the previous simulation were considered when choosing components based upon their power rating.

Another change to the circuit was utilizing the LTC7062 100V Dual High-Side MOSFET Gate Driver to drive the switches used in the converter. The two drivers are symmetric and independent of each other, allowing complementary or non-complementary switching [16]. Since the use of power MOSFETs impacts power loss in a converter significantly, they must be turned on and off quickly to minimize the transition time and power loss. Two LTC7062 devices were used in the circuit to drive the 4 N-Channel MOSFETs utilized in the converter design. Besides the addition of the driver, all other components were switched with real models except the transformer. When constructing the converter, one can add in parasitic components to the current transformer model such as leakage inductance, winding capacitances, coupling capacitances, and wire resistance if these values have been obtained from a datasheet. Figure 5-16 depicts the schematic of the proposed converter with mostly real models of the components.

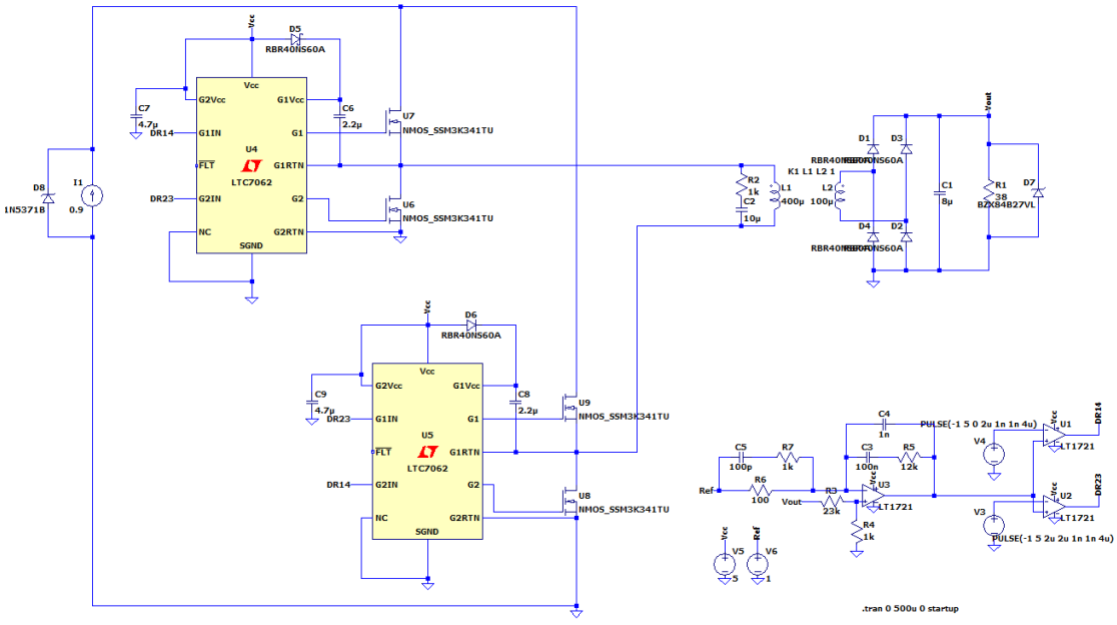

Figure 5-16. LTSpice Schematic of Proposed Converter with Mostly Real Components

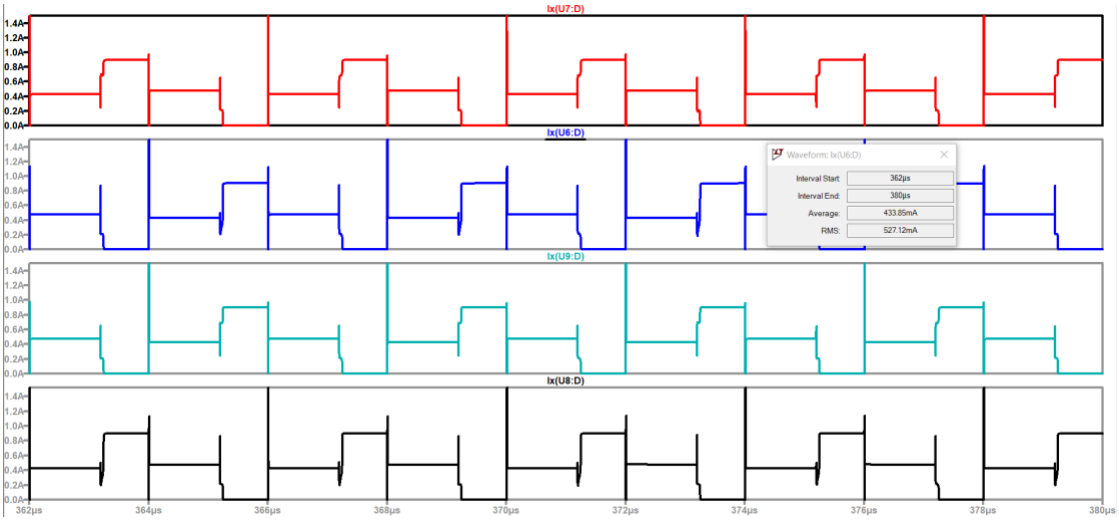

Figure 5-17. Switch Current Waveforms from Real Components Simulation

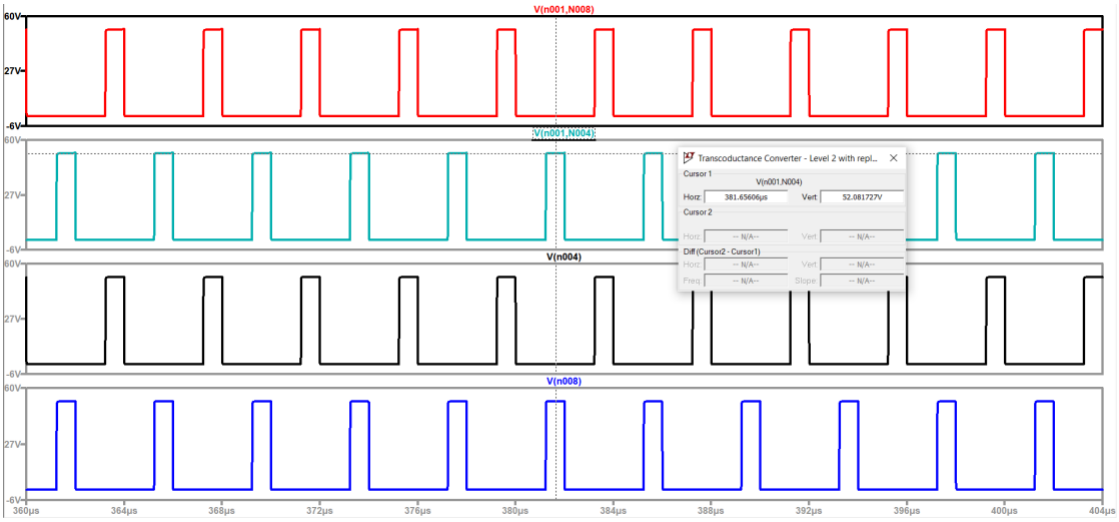

Figure 5-18. Switch Voltage Waveforms from Real Components Simulation

In Figure 5-17 it can be shown that the switch current waveform has the same general shape as seen in the original simulation, with a peak current of 0.9A, and an average current of 0.433A, which is 0.017A smaller than the expected value of 0.45A. However, one significant difference is that there are current spikes when each switch transitions from an on to off state or from off to on. In LTspice, these current spikes were measured to be 2.7A on switches S1 and S3 while switches S2 and S4 had current spikes of 4A and lasted for 6.95ns in total. This current spike was minimized from even larger

current values by utilizing an Schottky diode for D5 and D6. The peak switch voltage in Figure 5-18 was found to be 52.081V, which was 4.08V larger than the expected voltage of 48V. As mentioned previously, these differences have the most impact when choosing components for the converter as they should be rated to withstand both peak current and voltage values. Based on the potential for larger than expected peak currents on the primary side of the converter, each of these components should be rated for a minimum of 5A, if not more.

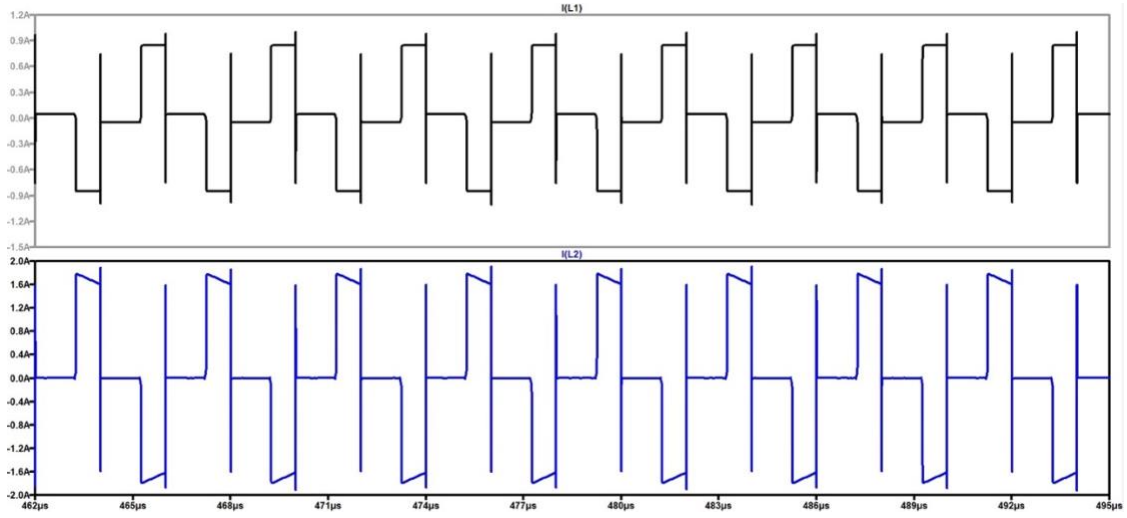

Figure 5-19 Primary and Secondary Inductor Currents from Real Components Simulation

Figure 5-19 displays the primary and secondary inductor current and this data shows that while both L1 and L2 currents are similar to those found with ideal currents, there are current spikes, particularly when moving from one level of current to another. It was found that average maximum current on the primary side is 0.9A with a peak of 0.99A, while the secondary side of the waveform has a maximum current of 1.93A, and an average value of 1.81A, which is close to the expected value of 1.8A. Similar to the current spikes found on the switches, these current spikes lasted for 7.9ns, then ended up stabilizing at the desired current.

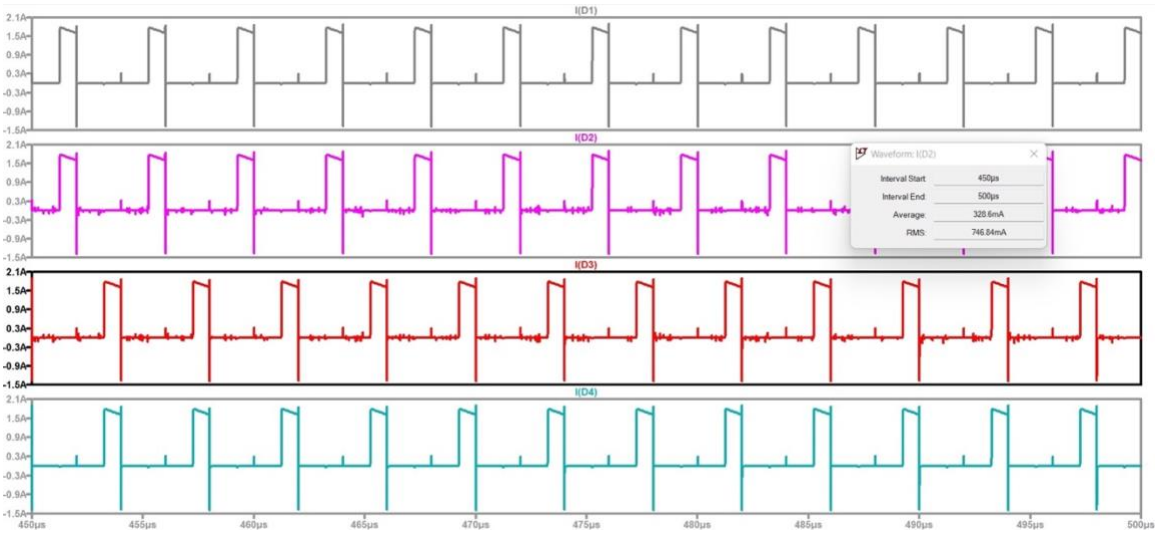

Figure 5-20. Diode Current Waveforms from Real Components Simulation

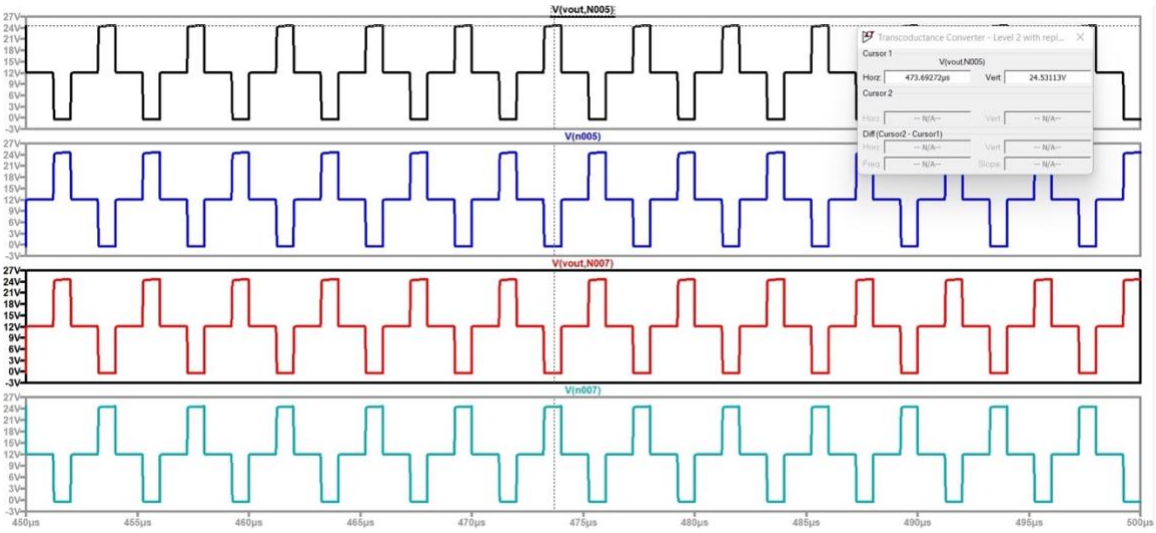

Figure 5-21. Diode Voltage Waveforms from Real Components Simulation

Figures 5-20 and 5-21 show the Diode Current and Voltage waveforms. The peak voltage through the diode was 24.53 V, with an average voltage value of 11.93V. This value was 0.53 V higher than the calculated value of 24V and this graph matched the results from the original simulation with ideal components. There are several discrepancies when looking at the diode current waveform. It is shown that there is a peak current of 1.78A and a current spike with a value of 1.87A when the waveform

switches from high to low that lasts for 8.12ns before stabilizing at 0A. Another difference is that there is a second current spike on the waveform which has a value of 0.315A for 8.13ns before stabilizing at 0A. This waveform had an average current of 0.328A, which was 0.015A larger than the calculated value of 0.313A. These current spikes could be due to the added components and non-idealities of the diodes chosen for the rectifier. They are also impacted by the initial current spikes seen in the switches on the primary side of the converter.

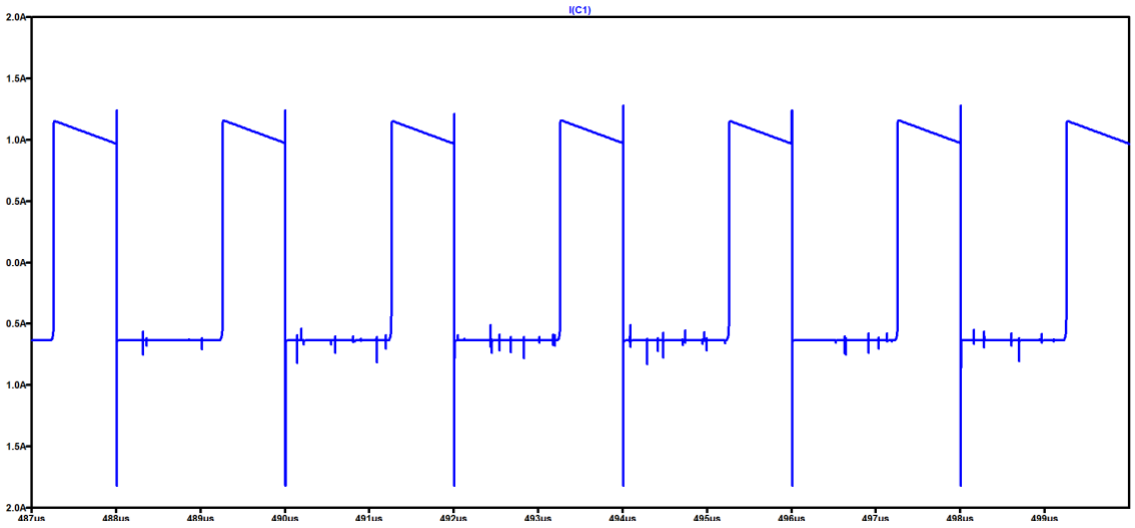

Figure 5-22. Output Capacitor Current Waveform from Real Components Simulation

An output capacitor of 8µF was utilized within the design. It was found that the peak current through the capacitor was 1.15A and the RMS current as 0.8337A, which was larger than the calculated value of 0.606A. These results were similar to those found in the first simulation model. As seen in previous waveforms, there is a current spike with a positive current of 1.2A and a negative current of -1.8A, before stabilizing at a value of -0.6A, lasting for 7.5ns.

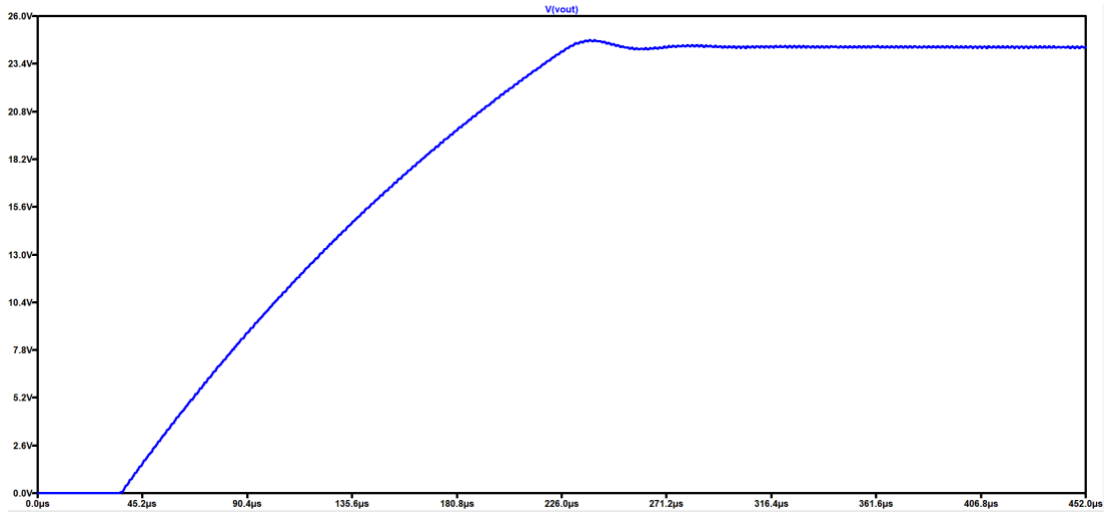

Figure 5-23. Output Voltage Waveform from Real Components Simulation

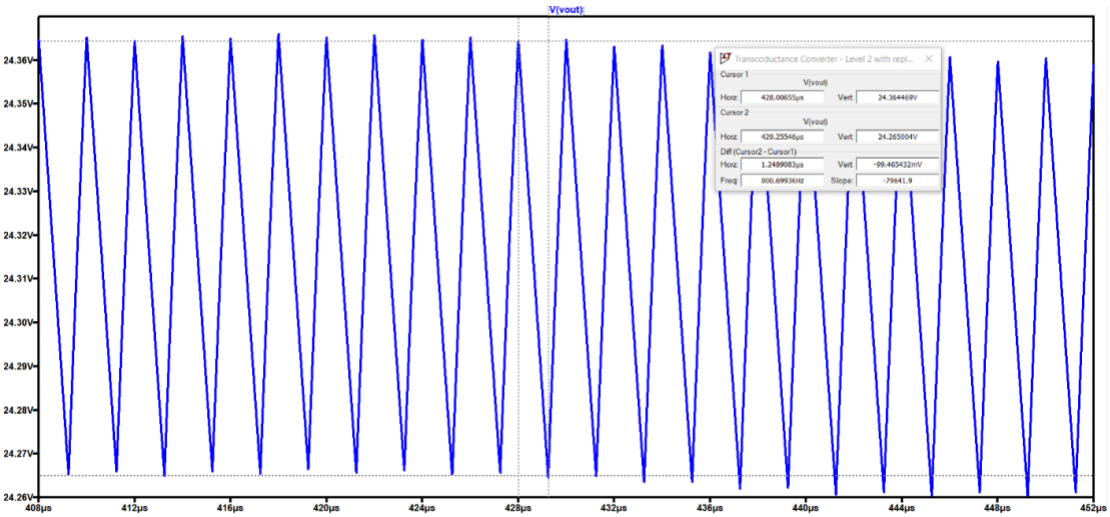

Figure 5-24. Output Voltage Peak to Peak Ripple from Real Components Simulation

Based on the results from Figures 5-23 and 5-24, it was found that $\bar{V}_{out}$ was measured to be 24.392V. The voltage peak to peak ripple (ΔV_o) was determined to be 0.099V, which matches with the expected result of 0.1V that comes with choosing an 8µF capacitor. This output voltage matches the requirements of the system as previously defined. Even with the current spikes found in the switches, transformer, and diode currents the overall output of the converter design still matches up fairly well to the desired results.

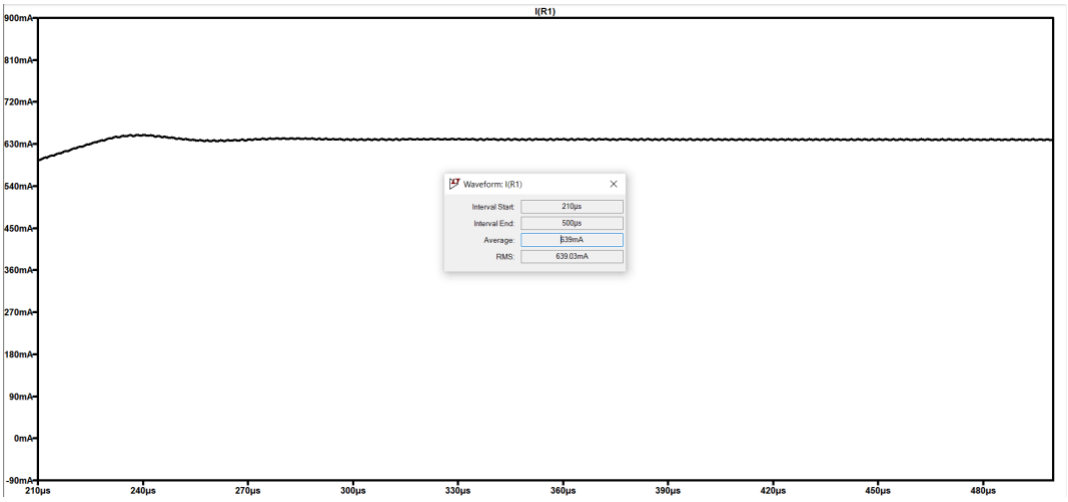

Figure 5-25. Output Current Waveform from Real Components Simulation

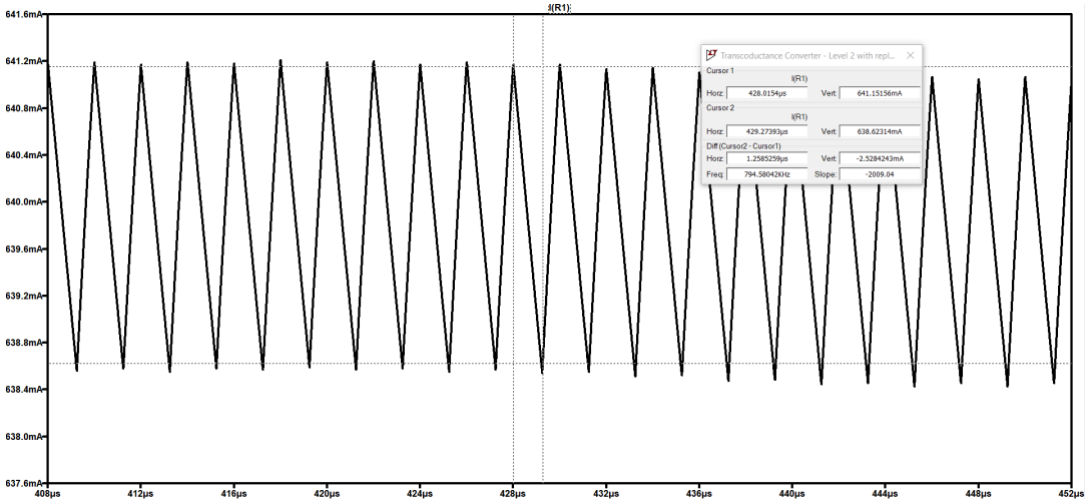

Figure 5-26. Output Current Peak to Peak Ripple from Real Components Simulation

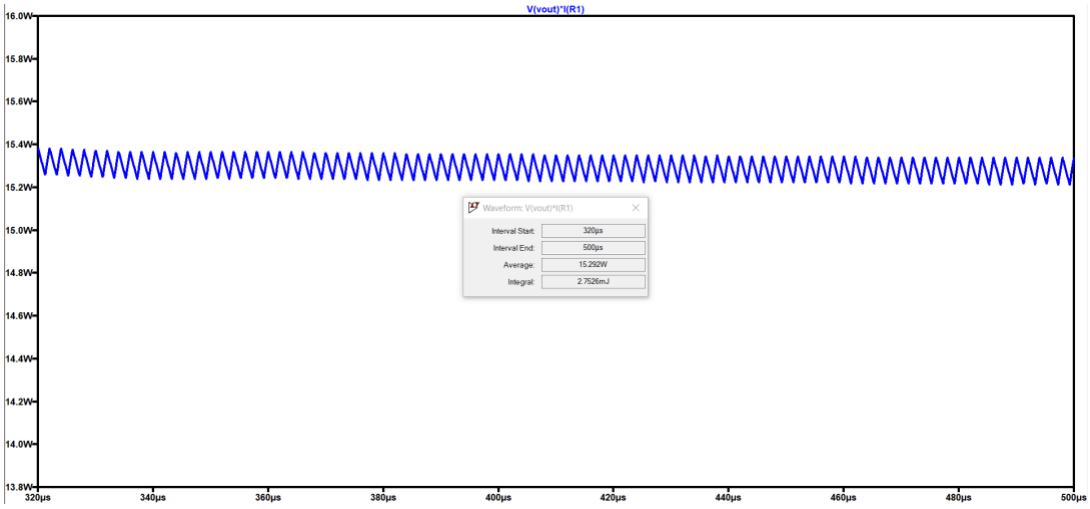

Figure 5-27. Output Power Waveform from Real Components Simulation

The results from Figures 5-25 and 5-26, show that $\bar{I}_{out}$ was measured to be 0.639A, which is larger than the desired current of 0.625A by 0.014A. It was also found that there was an output current ripple of 0.025A, which results in a peak-to-peak output current ripple of 3.96%. As shown in Figure 5-27, the output power was determined to be 15.292W, when the required output power was 15W, showing an increase of 0.292W, which is slightly under a 2% tolerance. The average input power into the system was determined to be 17.233W based upon the simulation results. By utilizing these two values, the overall efficiency of the converter was calculated to be 88.73%. A summary of the results of this simulation in comparison to the previous simulation results with ideal components can be found in Table 5-3.

Table 5-3. Comparison of Ideal Component Simulation vs Real Components Simulation

Parameter	**Ideal Components Simulated**	**Real Components Simulated**	**% Difference**
Average Switch Current	0.46 A	0.433 A	6.04 %
Peak Switch Voltage	51.4 V	52.08 V	1.31 %
Average Diode Current	0.318 A	0.328 A	3.09 %
Peak Diode Voltage	24.9 V	24.53 V	1.49 %
Average Output Current	0.634 A	0.639 A	0.78 %
Average Output Voltage	24.063 V	24.39 V	1.34 %
Average Output Power	15.289 W	15.292 W	0.196 %
I_{crms}	0.860 A	0.833 A	3.189 %
Output Voltage Ripple	0.101 V	0.099 V	2 %

The results from Table 5-3 display that the simulations with all ideal components had similar results overall to the simulation with mostly real components. The largest percent difference between the two simulations occurred in the average switch current value. However, when looking at the waveforms, there were several differences between

the current waveforms for all components in the design, and these differences must be taken into consideration when sizing and choosing the components. Even with this difference, the resulting output waveforms were close to what was expected, proving the feasibility of the design.

5.3 Final Comparison of Simulation Results

Table 5-4 shows the results of both simulations in comparison to the originally calculated values. From this data it can be determined that after placing real components into the design, the desired results of the DC-DC current-source converter were met. In both simulations, the largest differences occurred between the calculated values for I_{crms} and peak switching voltage. Overall, it was found that the results from simulation with ideal components most closely matched calculated values as expected. It should also be mentioned that the ideal components simulation had a higher efficiency of 93.5% while the real components simulation had an efficiency of 88.73%, which is still larger than the minimum efficiency of 80% as mentioned in the initial design specifications. Furthermore, the data from the initial simulation with ideal components, was found to be similar to the one with real components, further proving the feasibility of implementing this converter design in a real-world system.

Table 5-4. Comparison of Calculated Values to both Ideal Component Simulation Results and Real Components Simulation Results

Parameter	Calculated Value	Ideal Components Simulated Value	Real Components Simulated Value	% Difference Ideal vs Calculated	% Difference Real vs Calculated
Average Switch Current	0.45 A	0.46 A	0.433 A	2.19 %	3.85 %
Peak Switch Voltage	48 V	51.4 V	52.08 V	6.84 %	8.15 %
Average Diode Current	0.313 A	0.318 A	0.328 A	1.58 %	4.68 %
Peak Diode Voltage	24 V	24.9 V	24.53 V	3.68 %	0.54 %
Average Output Current	0.625 A	0.634 A	0.639 A	1.429 %	2.21 %
Average Output Voltage	24 V	24.063 V	24.39 V	0.262 %	1.611 %
Average Output Power	15 W	15.289 W	15.292 W	1.908 %	1.927 %
I_{crms}	0.606 A	0.860 A	0.833 A	34.65 %	31.5 %
Output Voltage Ripple	0.1 V	0.101 V	0.099 V	0.99 %	1.005 %

It is important to note that utilizing real components within the design impacted the current throughout the converter much more than the voltage. This observation can be verified by comparing the waveforms of each and noticing the spikes of current during changes of high to low or low to high current. In general, most of these spikes lasted between 6-8ns, with the longest irregularity lasting for 8.13ns. While these irregularities were present, it did not seem to affect the results of the output current or voltage in a significant way.

Chapter 6
CONCLUSION

The objective of this thesis was to provide a proof of concept for a current-source DC-DC converter to be utilized in underwater sensors that operate with low level DC electricity. The purpose of this converter is to step down an input current of 0.9A to 0.625A, while maintaining an output voltage of 24V and output power of 15W. This converter will serve as the input to a sensor located within an underwater submarine capsule, a component of an underwater communications system being developed by the Agency for the Assessment and Application of Technology in Indonesia.

An initial set of requirements were developed for the converter which included the desired output current, output voltage, output power, output voltage ripple, and efficiency. Analysis of the circuit was performed by deriving the transfer function of the current-source DC-DC converter design to relate the output voltage with the input current. The relationship between duty cycle, turns ratio, and input current was also investigated further. The results from the final simulation created in LTSpice demonstrate that the design was able to produce output current of 0.639A, output voltage of 24.53V, and output power of 15.292W. The efficiency of the converter and output voltage ripple were determined to be 88.73% and 0.4%, meeting original specifications of the design.

Some of the key differences between calculated and simulated results were found in the equations to size the ratings of the main power stage components. It was found that the previously estimated peak and average values for both voltage and current were slightly larger than expected within the simulation for all components. These results mean that the initial calculations for power ratings can be used as a good starting point

when choosing components, however one should expect slightly larger values when implementing the design and size components accordingly. Another issue found within the simulation were spikes of current during changes of high to low or low to high current. Each of these spikes lasted between 6-8ns, with the longest irregularity lasting for 8.13ns. These spikes were consistently seen in the switch, inductor, diode, and capacitor waveforms. To minimize these spikes, several different diode models were tested, and the one with the best results was chosen to be in the design. Despite these current spikes, the converter still had the desired output voltage, current and power results. Further work in reducing the amount or size of these current spikes could be one area of improvement within the future. This could be done by replacing the models for the gate driver, diodes, or other components with ones that result in a better outcome.

One area of improvement for this design could be developing a more realistic model of a transformer to be used within the simulation. Currently, the transformer utilizes 2 inductors and a coupling coefficient of 1. These values could be modified along with adding in leakage inductance, winding capacitances, coupling capacitances, and wire resistance if obtained from a datasheet of a transformer chosen for the design. This component would further affect the efficiency of the design, making the results even more realistic. Another area of improvement can come from preforming a study between switching frequency and efficiency to determine which switching frequency can create the most optimal results for the design. Overall, the proposed current-source DC-DC converter design serves as a proof of concept for creating a converter dependent on input current rather than voltage to achieve desired outputs. The system was successfully able to meet all the initial requirements and verified through simulations.

BIBLIOGRAPHY

[1]. S. O. Agbo and S. M. N. O., Principles of Modern Communication Systems. Cambridge, United Kingdom: Cambridge University Press, 2017.

[2]. M. Morris, “The Incredible International Submarine Cable Systems,” Network World, 19-Apr-2009. [Online]. Available: https://www.networkworld.com/article/2235353/the-incredible-international-submarine-cable-systems.html. [Accessed: 26-Oct-2021].

[3]. Tomoyuki, Kakehashi & Yoshinori, C. & Kaneaki, K. & Tomotaka, N.. (2010). Power feeding equipment for optical submarine cable systems. 5. 28-32.

[4]. Chesnoy Jose, Undersea Fiber Communication Systems, Elsevier ltd, 2016, pages 403-419

[5]. H. Nishikawa, H. Wakabayashi and M. Sato, "Power Feed Equipment for a Transoceanic Optical Fiber Submarine Cable System," INTELEC '87 - The Ninth International Telecommunications Energy Conference,1987, pp. 607-611

[6]. “What is Fiber Optics?,” The Fiber Optic Association. [Online]. Available: https://www.thefoa.org/foa.htm. [Accessed: 26-Oct-2021].

[7]. S. Lentz and B. Howe, "Scientific Monitoring And Reliable Telecommunications (SMART) Cable Systems: Integration of Sensors into Telecommunications Repeaters," 2018 OCEANS - MTS/IEEE Kobe Techno-Oceans (OTO), 2018, pp. 1-7, doi: 10.1109/OCEANSKOBE.2018.8558862.

[8]. Taufik, Introduction to Power Electronics, 3rd ed. Lulu Press, Inc. , 2020.

[9]. J. Falck, C. Felgemacher, A. Rojko, M. Liserre and P. Zacharias, "Reliability of Power Electronic Systems: An Industry Perspective," in IEEE Industrial Electronics Magazine, vol. 12, no. 2, pp. 24-35, June 2018, doi: 10.1109/MIE.2018.2825481.

[10]. O. Ambriz, “High Voltage DC-DC Converter Design for Submarine Application” San Luis Obispo, California

[11]. N. Bowers, “Voltage-fed or current-fed power topologies: A critical choice for users of multi-kw power sources,” Voltage- or current-fed power topologies: a critical choice, 15-Oct-2015. [Online]. Available: https://www.electronicspecifier.com/news/blog/voltage-fed-or-current-fed-power-topologies-a-critical-choice-for-users-of-multi-kw-power-sources?HQS=app-null-null-widget-ds-pf-ElectronicSpecifier-eu. [Accessed: 02-Dec-2022].

[12]. M. Mohebifar, N. Rostami, E. Babaei and M. Sabahi, "Dual-output step-down soft switching current-fed full-bridge DC-DC converter," 2017 14th International Conference on Electrical Engineering/Electronics, Computer, Telecommunications and Information Technology (ECTI-CON), 2017, pp. 773-776, doi: 10.1109/ECTICon.2017.8096353.

[13]. "LTspice," LTspice Simulator | Analog Devices. [Online]. Available: https://www.analog.com/en/design-center/design-tools-and-calculators/ltspice-simulator.html.

[14]. L. Cao, "Type III compensator design for power converters ," Jan-2011. [Online]. Available: http://caxapa.ru/thumbs/597674/Type3CompensatorDesign.pdf.

[15]. "LT1721," LT1721 Datasheet and Product Info | Analog Devices, 1998. [Online]. Available:https://www.analog.com/en/products/lt1721.html#:~:text=The%20LT1720%2FLT1721%20are%20UltraFast,with%20slow%20moving%20input%20signals.

[16]. "LTC7062," Datasheet and Product Info | Analog Devices, 2021. [Online]. Available: https://www.analog.com/en/products/ltc7062.html#product-documentation. [Accessed: 07-May-2022].